Title
Analysis of the pebble burnup profile in a pebble-bed nuclear reactor

Authors
Tang, Yushi
Zhang, Liguo
Guo, Qiuju
et al.

Publication Date
2019-04-01

DOI
10.1016/j.nucengdes.2019.01.030

Peer reviewed

Analysis of the pebble burnup profile in a pebble-bed nuclear reactor

Yushi Tang[a,c], Liguo Zhang[b], Qiuju Guo[a], Bing Xia[b], Zaizhe Yin[b], Jianzhu Cao[b], Jiejuan Tong[b], Chris H. Rycroft[c,d]

[a] *State Key Laboratory of Nuclear Physics and Technology, School of Physics, Peking University, Beijing 100871, People's Republic of China*
[b] *Institute of Nuclear and New Energy Technology, Collaborative Innovation Center of Advanced Nuclear Energy Technology, Tsinghua University, Beijing 100084, People's Republic of China*
[c] *Paulson School of Engineering and Applied Sciences, Harvard University, Cambridge, MA 02138, United States*
[d] *Mathematics Group, Lawrence Berkeley Laboratory, Berkeley, CA 94720, United States*

Abstract

In a pebble bed nuclear reactor, each fuel pebble draining through the core experiences a different amount of burnup depending on the precise trajectory that it follows. Understanding the burnup profile of pebbles is essential for reactor safety, as well as for fuel economy. Here, we introduce a method for constructing the burnup profile based on performing a discrete element simulation of the pebble drainage, followed by a burnup calculation in each individual pebble. This method is more accurate than previous approaches, and in particular it captures the extremal cases of pebble burnup. We demonstrate the method using the geometry, neutron flux data, and thermal characteristics from the HTR-10 reactor being developed at Tsinghua University. We examine pebble burnup during a single drainage cycle, and over multiple drainage cycles characteristic of normal reactor operation. Our results show that the presence of slow-moving boundary layers of pebbles near the reactor wall strongly influences the burnup profile. We perform a systematic study where the pebble–pebble and pebble–wall friction coefficients are independently varied, and we show that the strength of the boundary layers is a complex interplay of these two parameters.

Keywords: granular flow, pebble burnup, friction, burnup assay, fuel economy, reactor safety

1. Introduction

Nuclear energy is currently responsible for 10.6% of world electricity generation (IEA), and has seen a resurgence of interest in recent years by a variety of developing and developed countries (NEI News; Guo and Guo, 2016), driven in part by its advantages such as limited greenhouse gas production and resistance to price volatility in raw materials (Adamantiades and Kessides, 2009; Wang and Lu, 2002). There is currently a worldwide effort to develop Generation IV reactor designs, which aim to be safer and more efficient than existing technologies, with the goal of

Email addresses: ystang@pku.edu.cn (Yushi Tang), lgzhang@tsinghua.edu.cn (Liguo Zhang), chr@seas.harvard.edu (Chris H. Rycroft)

being commercially viable by 2020–2030 (Locatelli et al., 2013). One Generation IV design is the High-Temperature Reactor (HTR), which makes use of a graphite-moderated core and uses helium or molten salt as a coolant (IAEA-TECDOC-1198; IAEA-TECDOC-1674).

The pebble-bed reactor (PBR) is one type of HTR. The PBR core consists of a cylindrical vessel with a conical funnel at the bottom that is attached to an exit pipe (Fig. 1). The vessel is filled with 6 cm-diameter spherical TRISO fuel pebbles that have a graphite outer casing and contain uranium micropellets. During normal reactor operation, new pebbles are introduced at the top and drain very slowly through the core. When a pebble exits the core, the pebble burnup (characterized by the depletion of the nuclear fuel) is non-destructively assessed at a measuring site to determine whether the pebble should be recycled back into the core or be discharged to a waste storage facility (Fig. 1). This continuous refueling process requires no shutdown during operation, and is a major advantage of the PBR over other core designs. Helium gas is passed through the pebbles in the core to extract the generated heat, which is then sent into a heat exchanger. The PBR design has been studied by a variety of groups worldwide (Kissane, 2009). Examples include the prototype AVR reactor built in Germany (Gottaut and Krüger, 1990), and the PBMR project in South Africa (Koster et al., 2003; Ion et al., 2004; Venter and Mitchell, 2007). There is much interest in the PBR design in China: the HTR-10 is currently in operation at Tsinghua University (Xu and Zuo, 2002), and the first commercial demonstration project, the HTR-PM (High Temperature Reactor-Pebblebed Modules), is in development (Zhang and Sun, 2007; Zhang et al., 2009).

The slow, dense granular flow of pebbles through the core has many implications for reactor safety and efficiency, and has been studied extensively. Slow dense granular flows have surprisingly complex behavior, showing both solid-like and liquid-like characteristics (Aranson and Tsimring, 2002), and exhibiting discrete effects and inhomogeneities at the level of a single particle, such as extended force chains (Mueth et al., 1998; Utter and Behringer, 2004; Majmudar and Behringer, 2005). They have attracted much interest from physicists during the past two decades (Jaeger et al., 1996; Kadanoff, 1999), but so far no complete theoretical description exists. However, a variety of simplified continuum models have been proposed, especially for granular drainage, given its relevance to many industrial flows—examples include the kinematic model (Mullins, 1972, 1974), void model (Litwiniszyn, 1963; Caram and Hong, 1991), and spot model (Bazant, 2006; Rycroft et al., 2006a, 2010). Recently, advancements in granular continuum mechanics have been made (Jiang and Liu, 2003; Jop et al., 2006; Henann and Kamrin, 2013; Dunatunga and Kamrin, 2015), which have resulted in more realistic models across a variety of flows. An alternative approach is simulation using the Discrete Element Method (DEM), whereby each pebble is individually modeled according to Newton's laws (Cundall and Strack, 1979; Pöschel and Schwager, 2005). Due to the stiff interactions between granular particles, these simulations are computationally expensive, but are are well-suited to parallelization due to the local nature of the contact forces. DEM simulation has been used to study a variety of granular phenomena (Silbert et al., 2001; Landry et al., 2004; Depken et al., 2007), and has been shown to be in quantitative agreement with laboratory granular flows (Rycroft et al., 2009).

A combination of continuum modeling and DEM simulation has been used to study many aspects of granular flow in PBRs, including pebble velocity profiles and mixing (Rycroft et al., 2006b; Cogliati and Ougouag, 2006; Jiang et al., 2012), graphite dust generation due to frictional

wear at pebble–pebble contacts (Cogliati and Ougouag, 2008; Lind et al., 2010; Rycroft et al., 2012b,a; Stempniewicz et al., 2012), and the effects of the porosity properties of the pebble bed on the coolant flow (Ougouag et al., 2005; Hassan, 2008; du Toit, 2008).

In this work, we study how pebble flow affects the fuel burnup profile of the pebbles, and how it affects reactor safety and economical efficiency. Different pebbles take different times to drain through the core, and experience different neutron fluxes, thus resulting in inhomogeneous burnup. Furthermore, the measuring site has limited accuracy, meaning that some pebbles above the burnup threshold are recycled into the core, whereas some pebbles below the burnup threshold are discharged to the storage facility—both scenarios have safety implications (Tang et al., 2016). Previous approaches to study burnup have made use of the classical batch tracking method (Oppe et al., 2001; Gougar, 2004; Kim et al., 2008; Chen and Fu, 2014), where the core is divided into several axial flow channels. Each flow channel is then divided into several blocks, and software can assess the pebble burnup in each block. A major limitation of the batch-tracking method is that it neglects the differences in the burnup of different pebbles in the same block. This is an especially important issue near the vessel walls, where granular flows may exhibit boundary layers of slower flow (Rycroft et al., 2009), which could be missed if the region is homogenized.

Here, we take an alternative approach of performing DEM simulations of the pebble flow, and then computing the burnup of each pebble individually, by examining the irradiation history of its trajectory through the core. To the best of our knowledge, this approach has never been performed for PBRs, but provides much better accuracy of the burnup profiles, especially for pebbles in the boundary layers next to the walls. This allows us to characterize the the extremal cases of pebble burnup, which is of crucial importance for reactor safety. By computing the burnup of each pebble individually, we can also exactly model the burnup assay and the pebble recycling process, which allows us to quantitatively address the numbers of mis-recycled and mis-discharged pebbles. Our study requires that we compute the burnup profile of each pebble individually, which is more computationally expensive than existing approaches. However, we find that the workload is reasonable, and is substantially cheaper than running the DEM simulations themselves. Furthermore, since each pebble can be considered individually, the computation can be accelerated using multi-threading on a modern many-core desktop computer.

We base our study on the HTR-10 geometry (Wu et al., 2002), and make use of experimental neutron flux data (IAEA-TECDOC-1382). We examine the burnup of pebbles through a single cycle in the core, and we also model multi-cycle burnup, coupled with the burnup assay and recycling process. In normal operation, the neutron flux data shifts over time as the reactor passes through a variety of different states. To focus on the basic science of pebble burnup, we assume that the neutron flux remains constant. However, the computational tools developed here could easily be adapted to study a varying neutron flux history taken from an experimental facility.

In some cases, there is ambiguity about the appropriate DEM contact model parameters for simulating the interaction between pebbles. In particular, the frictional properties of graphite are known to vary greatly on the conditions, and limited data is available in the high-pressure, high-temperature, helium gas environment within the core. In a review article by Luo et al. (2010), friction coefficients ranging from 0.03–0.87 have been reported in the literature, with most lying in the range from 0.2–0.4. The effect of friction on granular flows has been addressed in a variety of

previous modeling studies. In work by Kamrin et al. (2007), simulations of a granular drainage in a wide silo (where the walls were of little importance) showed limited variation in flow profiles when the friction coefficient was varied over the range 0.1–0.9; it is hypothesized that this is because the packing geometry of how particles move and rearrange past one another is more important in determining the flow than the frictional contact forces. However, the situation is more complex when walls are present, and studies by Rycroft et al. (2006b) and Wang et al. (2013) have both shown that reducing wall friction results in a more uniform flow profile, with a much reduced boundary layer. Rycroft et al. (2012a) performed simulations of five different friction coefficients from 0.2 to 0.8, which showed substantial variations in the flow profile. However, in this study both the pebble–pebble and pebble–wall friction coefficients were set to be the same. Yang et al. (2012) compared DEM simulations to an experimental facility with glass beads, and examined the effect of friction, although again the pebble–pebble and pebble–wall friction coefficients were varied in unison, and the authors noted that friction plays a complicated role warranting further investigation.

Since friction properties affect the boundary layers, and hence the pebble burnup profiles, they are highly relevant to this study and we therefore examine their effect in detail. We present the results of a systematic study where both pebble–pebble and pebble–wall friction are varied independently. Our results are consistent with previous work, but provide a more complete picture of the role of friction, highlighting several different regimes. We show that the flatness of the velocity profile has a non-monotonic dependence on the pebble–pebble friction coefficient for certain pebble–wall frictions.

This paper proceeds as follows. In Section 2, we introduce the simulation methods that are used in the DEM pebble flow simulation in HTR-10 geometry. We then study the effects of the friction coefficients on the pebble flow regime in Section 3. Next, in Section 4, we introduce the burnup calculation process, and investigate the friction effects on the burnup profile of pebbles after one cycle. In Section 5, we construct the multi-cycle pebble burnup profile, and analyze the effects of the friction and the burnup assay accuracy. Finally, we conclude in Section 6.

2. Methods

2.1. Pebble contact model

The DEM simulations are performed using the Large-scale Atomic/Molecular Massively Parallel Simulator (LAMMPS) developed at Sandia National Laboratories (LAMMPS website; Plimpton, 1995). The code is widely used and provides a framework for simulating particles interacting under a diverse variety of forces. Here, we simulate spherical pebbles of diameter d interacting via a modified version of the contact model introduced by Cundall and Strack (1979). A natural simulation time scale is given by $\tau = \sqrt{d/g}$, where $g = 9.81$ m s^{-2} is the gravitational acceleration. For the pebble diameter of $d = 6$ cm, the time scale is $\tau = 0.0782$ s. The typical mass for a pebble in the HTR-10 is $m = 210$ g.

Consider two pebbles A and B, and let $\mathbf{r}$ be the separation vector from A to B. Define $\mathbf{n} = \mathbf{r}/\|\mathbf{r}\|$ to be the normal vector, and $\delta = d - \|\mathbf{r}\|$ to be the particle overlap. If $\delta > 0$, so that the pebbles are

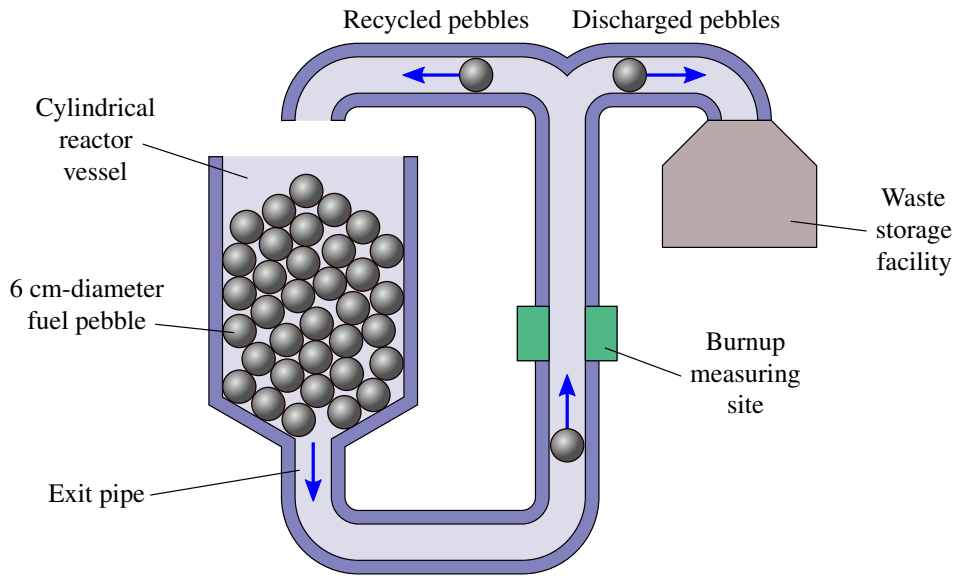

Figure 1: Schematic diagram of fuel circulation in a pebble-bed reactor. The reactor vessel (not shown to scale) is full of 6 cm diameter fuel pebbles that very slowly drain by gravity. Pebbles then flow out of exit pipe, after which the amount of fuel burnup is assessed at the measuring site. Each pebble is then either recycled back into the core, or discharged to a waste storage facility, depending on its amount of burnup.

in contact, then the normal and tangential components of the force on pebble A are

$$\mathbf{F}_n = f(\delta/d)\left(-k_n\delta\mathbf{n} - \frac{\gamma_n\mathbf{v}_n}{2}\right), \tag{1}$$

$$\mathbf{F}_t = f(\delta/d)\left(-k_t\mathbf{s}_t - \frac{\gamma_t\mathbf{v}_t}{2}\right), \tag{2}$$

respectively. Here, $k_{n,t}$ and $\gamma_{n,t}$ are the elastic and viscoelastic constants, respectively, and $\mathbf{v}_{n,t}$ are the normal and tangential components of the relative surface velocity. $\mathbf{s}_t$ is the tangential displacement at the contact point, integrated over the lifetime of the contact. The tangential force satisfies a Coulomb yield criterion $\|\mathbf{F}_t\| \geq \mu\|\mathbf{F}_n\|$ where μ is a friction coefficient. If $\mathbf{F}_t$ exceeds the criterion then it rescaled to have magnitude $\mu\|\mathbf{F}_n\|$, and $\mathbf{s}_t$ is recomputed in order to satisfy Eq. 2. The function f is defined as either $f(z) = 1$ for the Hookean contact model, or $f(z) = \sqrt{z}$ for the Hertzian contact model.

Table 1 shows the parameters that are used for this study, which are taken from Rycroft et al. (2012a). The Hookean contact model is used. For a detailed discussion of parameter choices the reader should consult Rycroft et al. (2012a) and Silbert et al. (2002). Pebble–wall contacts are handled using the same force model and parameters, except that the pebble–pebble and pebble–wall friction coefficients are set independently as μ_p and μ_w, respectively.

2.2. Simulations in the HTR-10 geometry

Throughout this study we make use of cylindrical (r,θ,z) coordinates with gravity pointing in the negative z direction. In the realistic HTR-10 geometry, there is an exit pipe of radius $r_{\text{exit}} = 4.17d$

Simulation parameter	Typical value
Normal elastic constant k_n	$2\times10^6 mg/d$
Tangential elastic constant k_t	$\frac{2}{7}k_n$
Normal viscoelastic constant γ_n	$50\sqrt{10}\tau^{-1}$
Tangential viscoelastic constant γ_t	$25\sqrt{10}\tau^{-1}$
Friction coefficient μ	0–0.5
Timestep	$2.5\times10^{-5}\tau$

Table 1: Typical values of the pebble contact model parameters used for the simulations in the paper.

at the base of the container, and we set $z=0$ to coincide with the bottom of the exit pipe. This connects to a conical funnel region which has a slope angled at 30°, and it extends from $z=2.5d$ to $z=8.75d$. The conical wall connects to a cylindrical wall of radius $r_{\text{cyl}}=15d$, which extends to $z=41.58d$ (Fig. 2(a)). The diameter of the fuel pebble is 6 cm. The total number of pebbles in the core is 27,000, with an average discharging flow rate of 125 pebbles per day.

The initial pebble packing is created by plugging the exit pipe with a horizontal wall at $z=2.5d$, and then randomly raining pebbles in from a height at a rate of 163.5 pebbles$/\tau$ (Landry et al., 2003). The packing is simulated until 1000τ until the particles come close to rest. After the initial pebble packing is constructed, the drainage simulations are carried out by removing the horizontal wall and letting the pebbles fall out under gravity. During drainage, snapshots of all pebble positions are outputted by LAMMPS at fixed time intervals of size 2τ. This data is subsequently post-processed by custom PERL scripts to perform the different analyses in this paper.

To mimic the continuous refueling process, pebbles that reach $z=0$ are randomly reinserted in the disk $z=42d, r<7.5d$ with downward velocity $3d/\tau$. These reinserted pebbles then resettle at the top of the pebble packing. Each drainage simulation was run for a duration $0\le t\le t_{\text{end}}$. Since the packing is initially stationary, our analyses are restricted to a time window $t_{\text{start}}\le t\le t_{\text{end}}$ to focus on the regime of continuous drainage. Unless otherwise stated, our simulations used $t_{\text{end}}=2000\tau$, and set t_{start} at the point when 120% of the total pebbles have been reinserted. For the analysis of the friction effects on the flow regime, discussed in Section 3, we performed initial packing and drainage simulations for each combination of μ_p and μ_w.

2.3. The effect of flow rate, and the construction of radial profiles

The flow rate under gravity for $\mu_w=\mu_p=0.3$ is 79.85 pebbles$/\tau$, which is much faster than the real reactor flow rate of 125 pebbles/day, by a factor of 7.06×10^5. Ideally, we would prefer to run full-size HTR-10 flow simulations at a real flow rate, but this is prohibitively expensive: since the simulation timestep must be kept constant in order to resolve pebble–pebble contacts, the required computational resources scale proportionally to the drainage time, and therefore scale inversely to the flow rate. However, previous experiments have shown that in slow, dense granular flows the overall flow rate has a weak effect on features of the flow, and results in an overall rescaling of time (Choi et al., 2004; Rycroft et al., 2009). Hence, as done in previous studies (Rycroft et al., 2006b, 2012a), we perform simulations at a faster flow rate, and then interpret the results at the physical flow rate by rescaling the time.

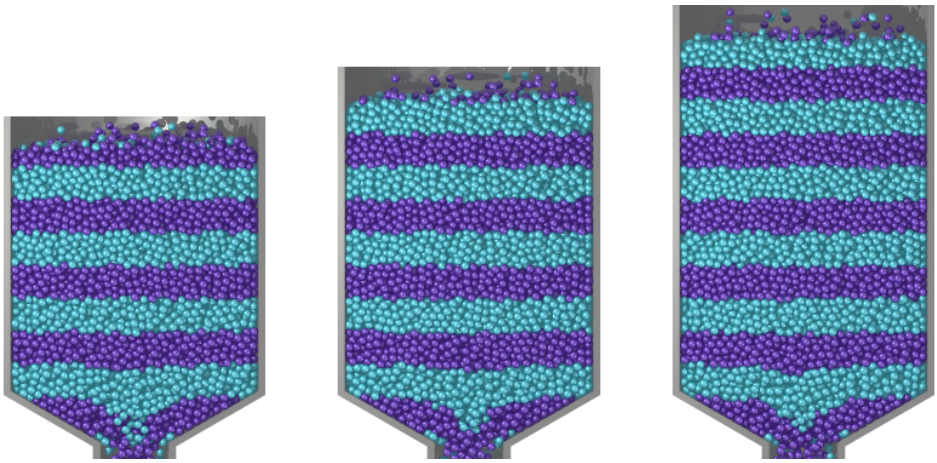

(a) (b) (c)

Figure 2: The draining snapshots after 8τ from the initiation of drainage in (a) the HTR-10 geometry, (b) the heightened geometry, and (c) the extended geometry, under the same friction $\mu_w = \mu_p = 0.5$. The pebbles are initially colored in horizontal stripes of width $4d$.

The slow, dense limit can be mathematically characterized as when the static stress σ^S (due to interparticle contacts (Christoffersen et al., 1981)) is much larger the kinetic stress σ^K (due to random particle motion (Silbert et al., 2001)). Previous work has shown that the ratio $\|\sigma^S\|/\|\sigma^K\|$ exceeds 100 in the bulk of the packing (Rycroft et al., 2012a), justifying the slow, dense regime. However, previous results also show that in the reinsertion region, σ^K is comparable to σ^S, and thus the rate could potentially affect the resettling of pebbles, which could in turn affect the structure of the packing in the bulk as those pebbles move downward over time. To investigate this, we performed a sequence of simulations where the flow in the exit pipe was restricted, by enforcing all pebbles under $z = 1d$ to have a fixed downward velocity. We measured the gravity-driven pipe velocity to be v_0. We then ran a sequence of simulations where the exit pipe velocity is scaled to v_0/λ where $2 \leq \lambda \leq 32$. Because the subsequent computations need to be done after the flow has completely stabilized, the draining duration for each of the simulation is different. For the larger values of λ, the value of t_{end} is increased. Ideally, t_{end} should be increased proportionally to λ, but due to the extreme length of the simulations this was infeasible. For our maximum value of $\lambda = 32$, we used $t_{\text{end}} = 17752\tau$. We checked that our comparisons for different values of λ were not sensitive to the precise time window chosen.

Throughout the paper, we plot a number of profiles of different fields along the radial coordinate, and we make use of the following binning procedure adapted from Rycroft et al. (2006b) and Rycroft et al. (2012a). Let $R(z)$ be the radius of the reactor as a function of z, and consider all pebbles with positions (r_k, z_k) over the analysis interval $t_{\text{start}} \leq t \leq t_{\text{end}}$ whose vertical position lies within a certain height range, $|z_k - z_{\text{mid}}| < h$. For each pebble, we first construct a rescaled radius $s_k = r_k R(z_{\text{mid}})/R(z_k)$. In the cylindrical section of the reactor, this rescaling has no effect. However, in the conical section, this helps ensure that any fine features in the profile that are aligned with the conical wall are resolved.

We then bin the pebble quantity of interest (*e.g.* pebble velocity, pebble spin) in bins that are of

equal size in $(s_k)^\alpha$ for some exponent α. This nonlinear binning is used because in the cylindrical geometry there are proportionally more pebbles at larger radii; specifically, the number of pebbles in a bin of size Δr located at radius r will be proportional to $r\Delta r$. Consequently, the standard deviation in the measurement in this bin is proportional to $(r\Delta r)^{-1/2}$. If Δr is constant, this results in very high accuracy near the reactor wall, and poor accuracy near the reactor center. Instead, we choose the standard deviation to be proportional to the bin size, so that $(r\Delta r)^{-1/2} \propto \Delta r$. and hence $\Delta r \propto r^{-1/3}$. This, in turn, implies an exponent of $\alpha = 4/3$.

The LAMMPS code internally tracks the instantaneous velocity of every pebble, but we do not store this information since it substantially increases the size of the output data. Instead, to construct a velocity profile, we compute pebble velocities from two successive timesteps. If a pebble is at position $\mathbf{x}_n$ at time t_n and $\mathbf{x}_{n+1}$ at time t_{n+1} then we treat it as having position $(\mathbf{x}_{n+1}+\mathbf{x}_n)/2$ with velocity $(\mathbf{x}_{n+1}-\mathbf{x}_n)/(t_{n+1}-t_n)$, and use the binning procedure described above.

Figure 3(a) shows the average number density distribution in the region $25d < z < 35d$ as a function of r, for six different flow rates. Next to the wall the pebbles are ordered into well-defined layers, which become progressively less clear into the bulk (du Toit, 2002, 2008; Rycroft et al., 2009). The curves almost overlap, indicating that the effect of the flow rate is small. To further analyze the differences, Fig. 3(b) shows the average volume fraction in the region $25d$–$35d$ as a function of flow rate. There is a small but clear trend for simulations at lower flow rates to pack at slightly higher density. However, the differences appear to saturate, with minimal alteration between $\lambda = 16$ and $\lambda = 32$. The data points are well fit by the function

$$\phi(\lambda) = 0.6117 - 0.0106 \times \lambda^{-1.376}. \tag{3}$$

We therefore estimate that the difference between the gravity flow and the real flow will be $\phi(1) - \phi(7.06 \times 10^5) = 0.0106$, which we consider small enough to neglect. Figure 3(c) shows that the flow rate has no obvious impact on the rescaled velocity profiles, providing justification for the time rescaling procedure discussed at the start of this section.

2.4. Simulations in the heightened geometry

Due to the enhanced pebble motion at the top of the packing, the individual pebble trajectories in the simulation are quite different from a flow at the physical drainage rate. To investigate this further, Fig. 4 shows two scatter plots of the correlation between radial positions at different heights H, $3H/4$ and $2H/4$, where H is the height of the HTR-10. Figure 4(a) shows that pebble radial positions change substantially from H to $3H/4$; in addition, the plot shows that pebbles move radially outward, as they tumble down the top of the packing. However, Fig. 4(b) shows that the radial position of pebbles remains stable from $3H/4$ to $2H/4$. Once they enter the bulk of the pebble packing, they mainly move vertically downward. In the subsequent analyses of the pebble flow, we therefore focus attention on the region where z is less than $z_c = 3H/4$, where the pebble trajectories have stabilized. In this region, we expect the results will match well to the real geometry at the physical flow rate.

To quantitatively analyze the pebble burnup, we cannot restrict attention purely to the region $z < z_c$. While neutron fluxes are generally highest in the center of the reactor, and lower in the periphery, we expect that the region where $z \geq z_c$ will still have an appreciable contribution to the

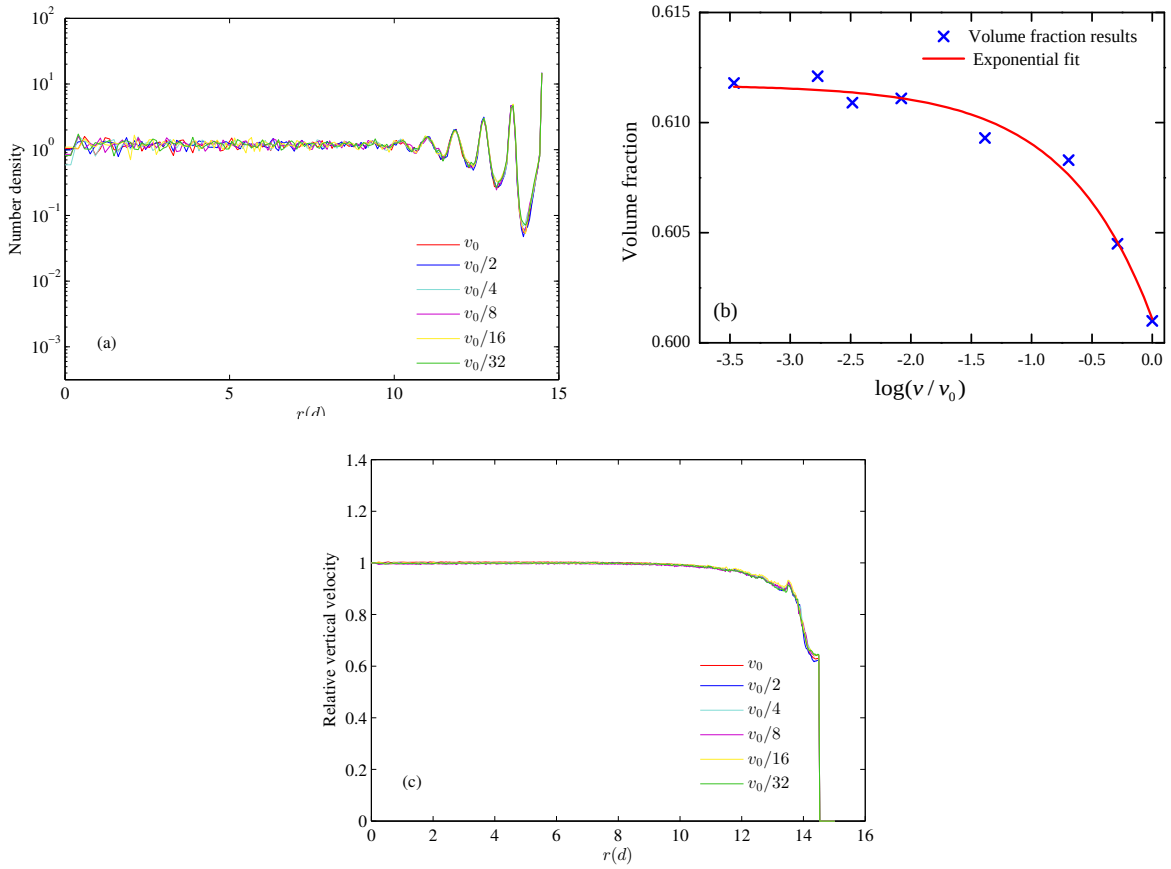

Figure 3: (a) The average number density distribution along the radius, (b) the average volume fraction with exponential fit, and (c) the average relative vertical velocity, averaged over the range $25d < z < 35d$, using $\mu_p = \mu_w = 0.3$. Here, v_0 is the average vertical velocity in the exit pipe under gravity-driven flow. The runs for fractional v_0 are based on artificially controlling the exit pipe velocity to be slower.

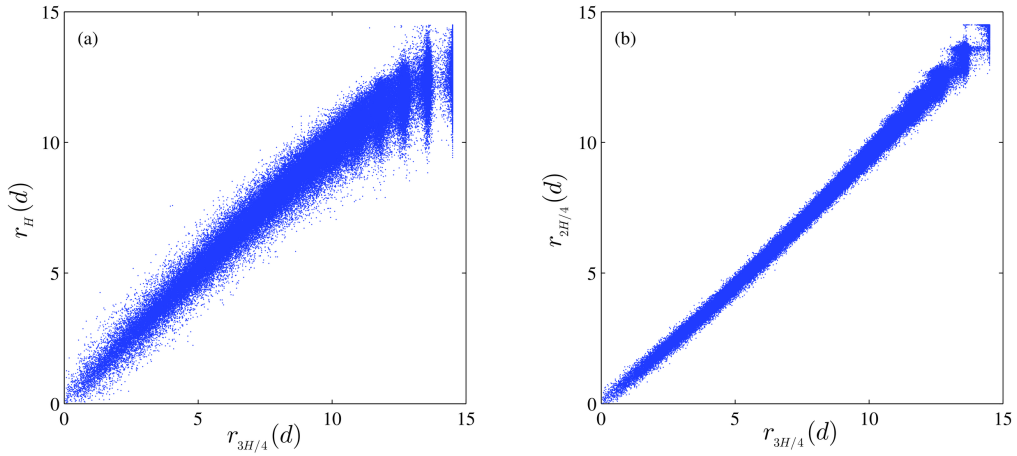

Figure 4: Scatter plot of pebble radial positions at (a) $z = H$ and $z = 3H/4$ and (b) $z = 2H/4$ and $z = 3H/4$, where H is the height of the HTR-10 geometry.

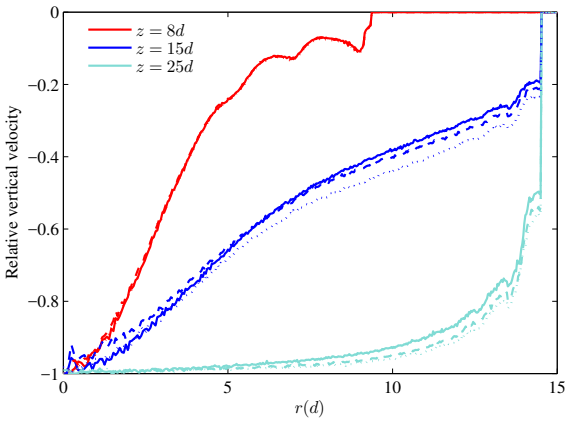

Figure 5: Vertical velocity at different heights in three different geometries using the same friction parameters $\mu_w = \mu_p = 0.5$. The solid line, dashed line, and dotted line are for the HTR-10, the heightened, and the extended geometry, respectively.

pebble burnup. However, as mentioned above, the pebble trajectories in this region are not a good match to the physical flow.

Based on these considerations, we introduced a heightened HTR-10 geometry. The original height of HTR-10 is set to be the $3/4$ of the new heightened geometry. Thus the original height of the active zone in the core is heightened from $36d$ to $48d$. For validation purposes, an extended geometry with height $56d$ is also introduced. Table 2 lists the simulation parameters for these two modified geometries, as well as some details about the computations. Figure 2 shows the drainage snapshot for the different geometries. In the subsequent burnup calculations, we therefore focus on the heightened geometry, and examine pebble trajectories in the region $z < z_c$ where $z_c = 3(48d)/4 = 36d$ in this case. These trajectories match the height of the original HTR-10 geometry, without the transient mixing effects in the top of the packing.

A possible concern with the heightened geometry is that the additional pebbles could affect the velocity field in the bulk of the packing. However, the Janssen effect (Janssen, 1895; Sperl, 2006) shows that the weight of a tall granular column is supported by friction with the wall. Hence, beyond a certain height, the stress distribution in the column saturates and the stresses near the exit pipe are similar, so the velocity profiles are similar. This is confirmed in Fig. 5, which shows velocity profiles at several heights for the three different geometries.

3. Friction effects on the flow regimes

We now examine the effect of friction on the pebble flow, which has important consequences for pebble burnup. Previous studies have examined the role of friction (Kamrin et al., 2007; Rycroft et al., 2012a; Yang et al., 2012), but here we systematically vary both the pebble–pebble friction coefficient μ_p, and the pebble–wall friction coefficient μ_w.

Figure 6 highlights a surprising non-monotonic behaviour as the friction properties are varied. Three snapshots with μ_w fixed to 0.2, and $\mu_p = 0.01, 0.125, 0.5$ are shown, where the pebbles are

Simulation parameter	HTR-10	Heightened	Extended
Number of pebbles	27000	31500	37500
Pebble insertion height	$42d$	$48d$	$56d$
Trajectory start height z_c	$31.5d$	$36d$	$42d$
Drainage time	2000τ	2500τ	3000τ
Number of processes	72	72	38
Computation time	21.08 s/τ	23.19 s/τ	34.66 s/τ

Table 2: Simulation parameters and computational details for the three geometries considered in the three geometries. Computation time is measured in terms of the wall clock time required to compute one unit of simulation time.

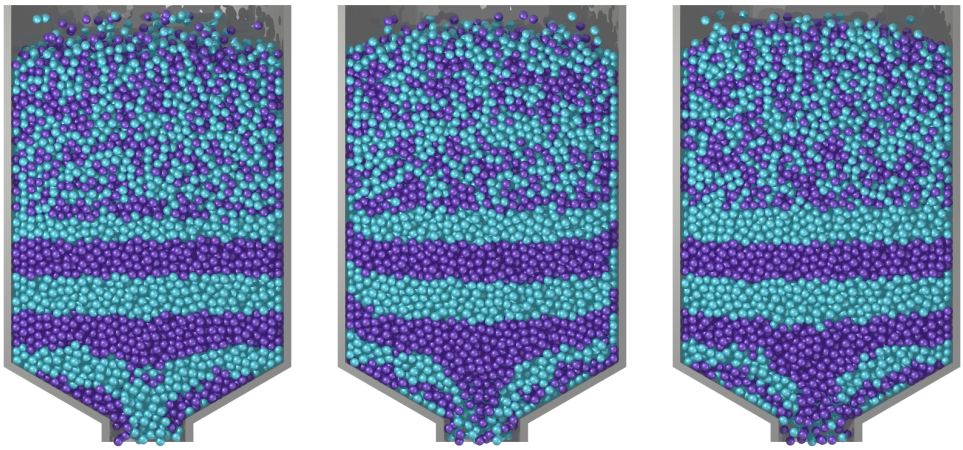

(a) (b) (c)

Figure 6: Snapshots of the steady flow regime with $\mu_w = 0.2$ for different pebble friction: (a) $\mu_p = 0.01$, (b) $\mu_p = 0.125$, and (c) $\mu_p = 0.5$. The pebbles are initially colored in horizontal stripes of width $4d$. The snapshots are shown after the 110τ, 162τ, and 214τ, which corresponds to approximately the same total amount of pebble flow for each simulation.

colored in stripes according to their initial z coordinate. For the smallest friction, $\mu_p = 0.01$, the interfaces between colored layers are almost horizontal, showing that the pebbles fall like a plug. For $\mu_p = 0.125$, a boundary layer of slower pebble flow is visible, but this disappears for $\mu_p = 0.5$. To understand this phenomenon in more detail we performed a suite of simulations where both μ_p and μ_w are varied. We focused on the range of friction coefficients from 0.01–0.5, which encompasses the bulk of experimental measurements presented by Luo et al. (2010).

To capture the size of the boundary layer, we define R_v to be the ratio between the boundary velocity and the central velocity at a certain height. Figure 7 shows R_v at different heights as a function of μ_p, for four different values of wall friction ($\mu_w = 0.1, 0.2, 0.3, 0.5$). R_v generally increases with height, since the velocity profile becomes more plug-like. For $\mu_w = 0.2$, strong non-monotonic behavior in R_v is visible, which is consistent with the snapshots in Fig. 6; in fact, the snapshot of Fig. 6(b) where $(\mu_w, \mu_p) = (0.2, 0.125)$ corresponds to the trough in Fig. 7(b) where the non-monotonic behaviour is the strongest. However, non-monotonic behavior is visible across a range of μ_w values.

To understand the non-monotonicity in more detail, we examined the spin of the pebbles. We

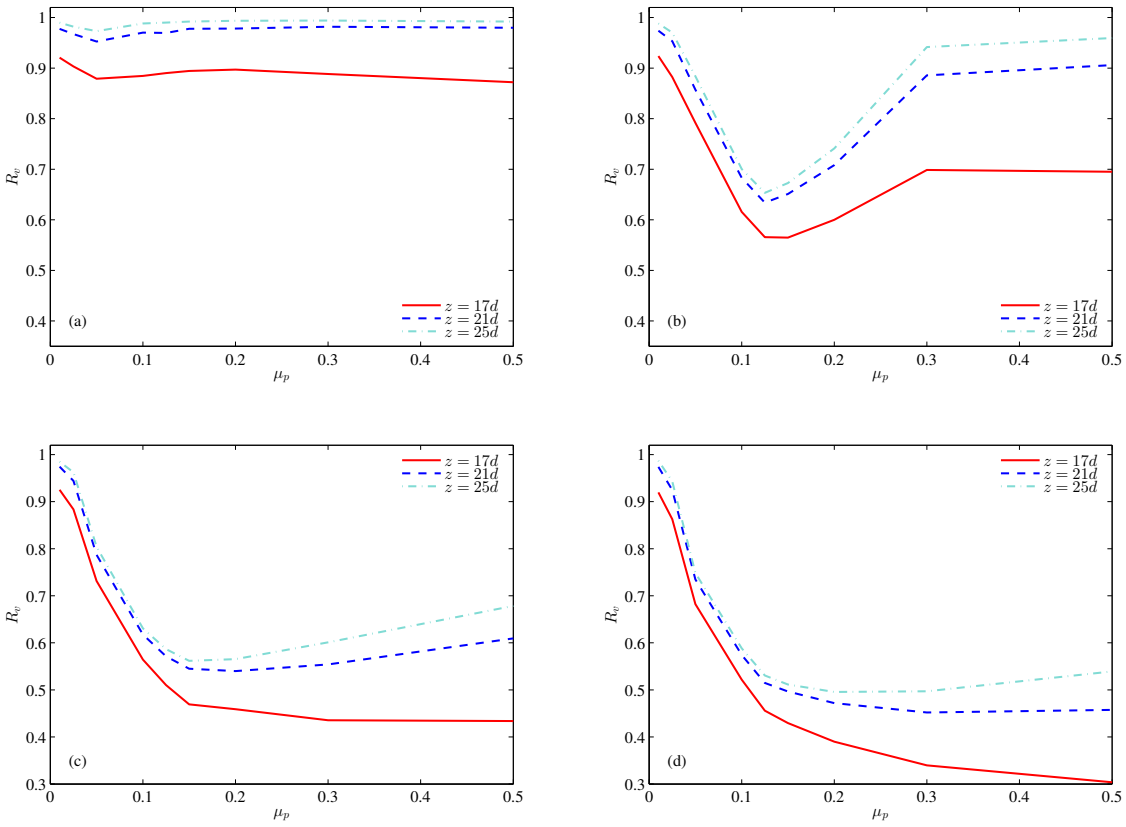

Figure 7: The R_v value as a function of pebble friction μ_p, at different heights under different wall friction: (a) $\mu_w = 0.1$, (b) $\mu_w = 0.2$, (c) $\mu_w = 0.3$, and (d) $\mu_w = 0.5$.

obtained the angular velocity vector ω for each pebble from LAMMPS, and we converted it into the cylindrical coordinate system $\omega = (\omega_r, \omega_\theta, \omega_z)$. Due to the rotational symmetry of the HTR-10 geometry, the long-term time averages ω_r and ω_z will be zero. However, ω_θ can have a non-zero long-term time average and provides useful information about how pebbles roll against the wall. Figure 8 shows time-averaged plots of ω_θ for the three cases in Fig. 6.

The figure shows that the $\mu_p = 0.01$ case (Fig. 8(a)) has the highest pebble spin. Next to the wall, a thin layer of negative ω_θ is visible, which is shown more clearly in Fig. 9 where ω_θ is plotted as a function of r. Since the friction with the wall is much greater than the friction between pebbles, the pebbles will roll down the wall. Due to low pebble–pebble friction, the pebbles can easily rotate past each other. Hence, overall the pebbles can flow like a plug, but individual pebbles are spinning and there substantial relative motion at each pebble–pebble contact.

For $\mu_p = 0.125$ (Fig. 8(b)) the situation is different. The pebbles next to the wall still spin due to their contact with the wall, but due to enhanced pebble–pebble friction, the adjacent pebbles can no longer easily slide against each other, and therefore a boundary layer forms. For $\mu_p = 0.5$ (Fig. 8(c)) very little spin is visible next to the wall. In this case, the pebble–pebble friction is strong enough that the pebbles fall as a rigid plug, with limited sliding at each pebble–pebble contact. The

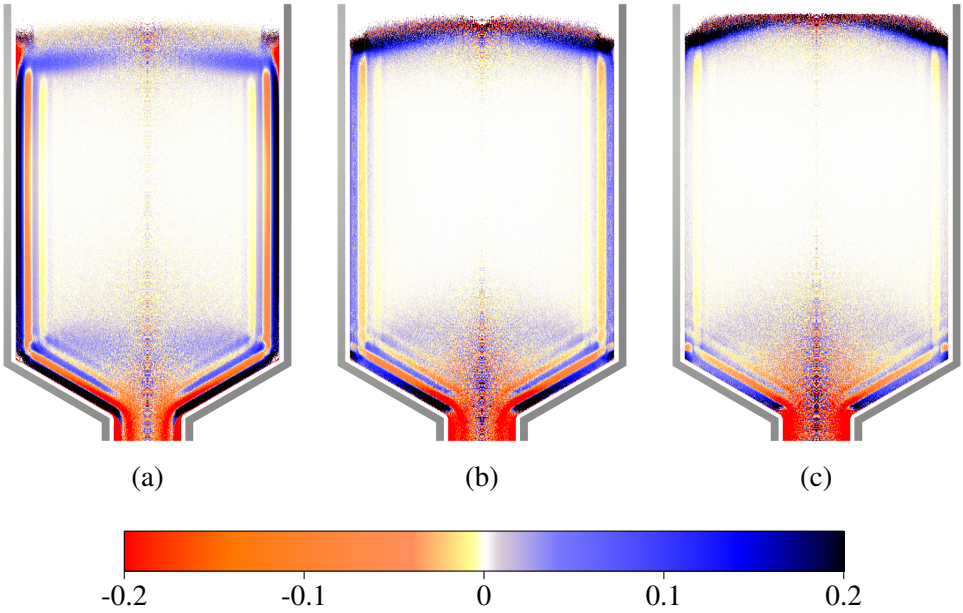

Figure 8: Plots of the time-averaged pebble angular velocity component ω_θ (with units of $1/\tau$)in the core with $\mu_w = 0.2$, under different pebble friction: (a) $\mu_p = 0.01$, (b) $\mu_p = 0.125$, and (c) $\mu_p = 0.5$.

	$\mu_p = 0.01$	$\mu_p = 0.1$	$\mu_p = 0.2$	$\mu_p = 0.3$	$\mu_p = 0.5$
$\mu_w = 0.1$	145.74	106.93	92.13	84.83	77.64
$\mu_w = 0.2$	145.46	104.31	88.03	80.47	74.47
$\mu_w = 0.3$	145.04	104.01	87.85	79.85	73.07
$\mu_w = 0.5$	144.86	103.49	87.41	79.44	72.43

Table 3: Average discharge rates for different pebble and wall friction coefficients, given in units of pebble$/\tau$.

pebbles in contact with the wall slide against it, as opposed to rolling along it. This is confirmed in Fig. 9 where ω_θ is almost zero for this case.

We also created a color plot of R_v as a function of μ_p and μ_w for several different heights (Fig. 10), providing another viewpoint on the non-monotonicity. In addition, Table 3 shows the flow discharge rate as a function of the friction coefficients. The flow rate increases as both friction coefficients are lowered, but the dependence on wall friction μ_w is stronger. Overall, our results show that both pebble and wall friction strongly affect the flow regime in the core. We bear these results in mind as we proceed to examine the pebble burnup characteristics.

4. The pebble burnup profile after one drainage cycle

4.1. Construction and validation of the pebble trajectory database

The amount of burnup that a pebble experiences is based on its trajectory through the core. Therefore, for the subsequent analysis, we build a pebble trajectory database—each trajectory consists of snapshots of a pebble position from $z = z_c$ until it exits the core.

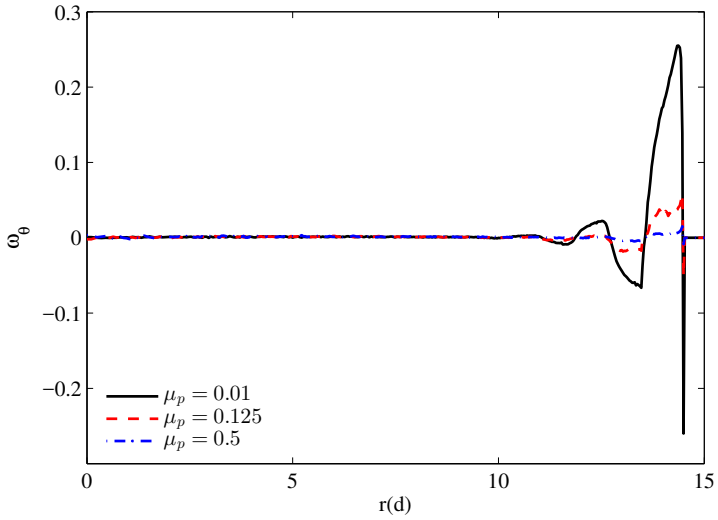

Figure 9: The average ω_θ over the range $15d < z < 25d$ as a function of the radial coordinate, using $\mu_w = 0.2$ and three different values of pebble–wall friction coefficient μ_p.

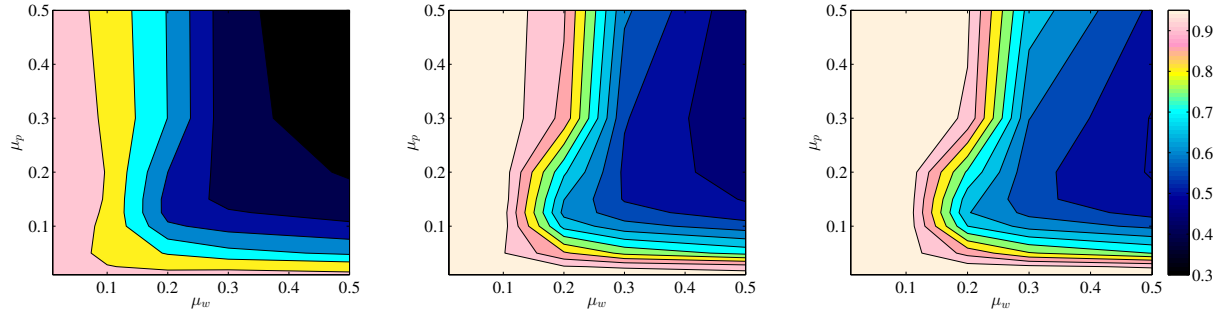

Figure 10: Color plots of R_v (the ratio of boundary z velocity to center z velocity) as a function of both pebble and wall friction at (a) $z = 17d$, (b) $z = 21d$, and (c) $z = 25d$.

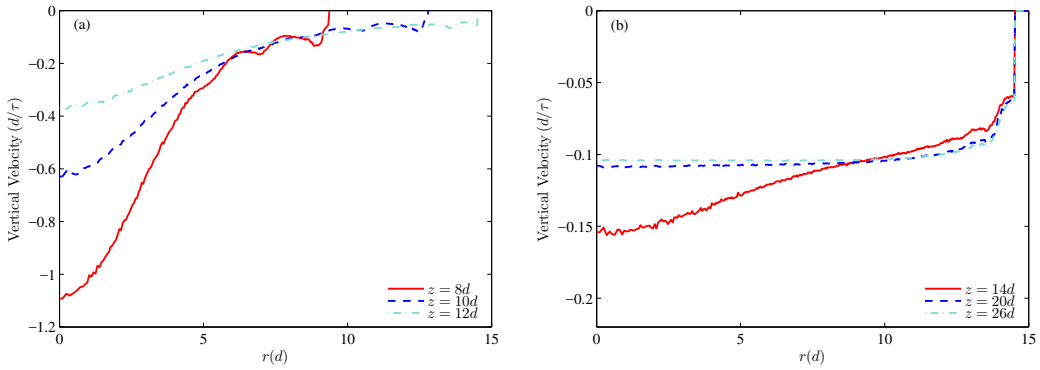

Figure 11: Vertical velocity profiles at different heights in (a) the converging region and (b) the middle of the core, for $\mu_p = \mu_w = 0.3$ in HTR-10 geometry.

It is important to choose the trajectories in the right proportions to be reflective of the real pebble flow. If we considered all pebble trajectories over our simulation time window, $t_{\text{start}} \leq t \leq t_{\text{end}}$, then we would preferentially sample trajectories of a shorter duration, since more will fit into this window. Instead, we first determine a cutoff maximum duration of a trajectory, T, which we determine empirically. We then take a random sample of trajectories that begin in the interval $t_{\text{start}} \leq t \leq t_{\text{end}} - T$. All of these trajectories will complete by the end of the simulation window. For the analyses presented in this paper, we compile approximately 60,000 trajectories into the database.

To verify that our trajectory database samples pebbles in the correct proportions, we perform a validation by computing the residence time of pebbles to pass from $z = z_c$ to the exit pipe in the heightened HTR-10 geometry, using $\mu_w = \mu_p = 0.3$. Each pebble trajectory has on average 150 time points. The vertical velocity profiles for this case are shown in Fig. 11. In the lower parts of the geometry (Fig. 11(a)) the velocity field converges toward the exit pipe. In the upper region (Fig. 11(b)) the flow becomes plug-like, although for these choices of friction there is a boundary layer of slower pebbles next to the wall. Figure 12 shows the residence times of pebbles as a function of their initial radial coordinate at $z = z_c$, scaled according to the physical flow rate. Pebbles inserted near the center (*i.e.* $r = 0$) have the shortest residence times. As r increases, the residence time increases. In particular, the graph shows that pebbles inserted next to the wall have a considerably longer residence time, with some taking up to 400 days to drain through the core. The average pebble residence time is 207 days, which closely matches the expected value for the HTR-10.

4.2. The burnup calculation

We perform the burnup calculations using the program KORIGEN (Karlsruhe version of Oak Ridge Isotopes Generation and Depletion Code), developed by German KfK nuclear research center (Fischer and Wiese, 1983; Matsson, 1995). The code calculates the nuclear isotope generation, depletion, burnup, radioactivities of nuclear fission reactor fuels in nuclear reactors like the HTGR (High-Temperature Gas-cooled Reactor), LWR (Light-Water Reactor), and MSBR (Molten Salt Breeder Reactor). We use KORIGEN as a black box to calculate the burnup history in each pebble. We provide KORIGEN with the mass of the fuel in the pebble (the fuel enrichment in the pebble is

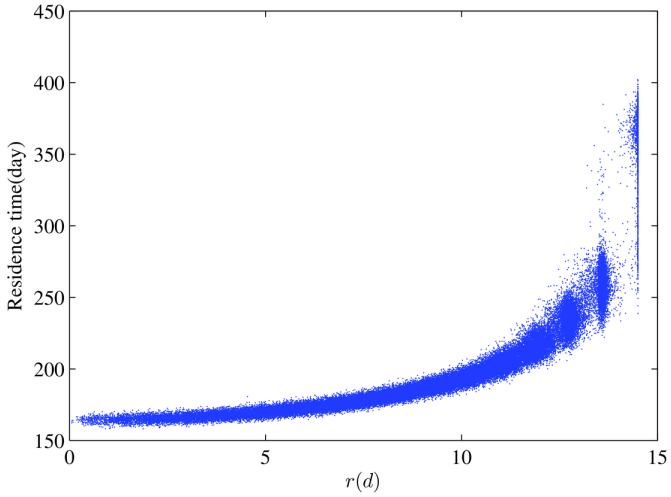

Figure 12: Scatter plot of the pebble residence time along the radius r of HTR-10 geometry for $\mu_p = \mu_w = 0.3$.

17%), and the time history of the neutron flux and temperature that the pebble experiences. The key information we need from its output file is the burnup and radioactivities of the burnup indicator, Caesium-137 (Cs-137), in each pebble. The burnup is defined as the energy released per mass of fuel, and its units in the paper are gigawatt days per ton of uranium (GWd/tU). During normal reactor operation, the neutron flux may vary significantly over time. Here, for simplicity, we restrict to neutron flux and temperature data obtained during 10 MW steady operation of the HTR-10, as shown in Fig. 13.

To perform the burnup calculations, we make use of a pebble trajectory database, which was introduced previously. For a given trajectory, we create a KORIGEN input file consisting of equally-spaced time points, and the corresponding neutron flux and temperature data. The neutron flux and temperature data are based on bilinear interpolations of the HTR-10 data shown in Fig. 13, using the pebble's (r,z) position. Typically, it takes less than five seconds to run a KORIGEN input file for one complete drainage cycle through the reactor. We ran our analysis program on a desktop computer with dual 2.20 GHz 10-core Intel Xeon E5-2630 v4 CPUs. Using hyper-threading, allowing for two threads to run per physical core, our analysis program forked up to forty copies of KORIGEN to run simultaneously. This allowed us to process hundreds of thousands of pebble burnup histories within several hours. No modifications to LAMMPS are required and the burnup calculations are performed entirely by post-processing the standard LAMMPS output data.

We use KORIGEN to calculate the burnup at each timestep in the pebble history, and the activity of the target nuclide Cs-137 at the bottom. Cs-137 is one of the most important indicators of the burnup measurement. In the following section, we examine the burnup profile in the core itself. We then examine the final burnup profile for pebbles that have completed a full drainage cycle. In both sections we examine the role of pebble friction ($\mu_p = 0.05, 0.125, 0.2, 0.5$) and wall friction ($\mu_w = 0.1, 0.2, 0.3, 0.5$).

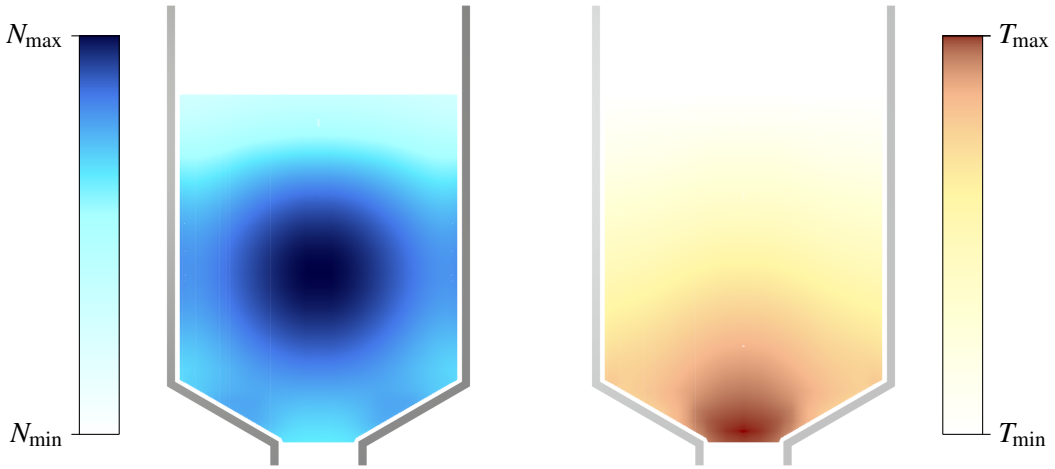

Figure 13: Typical distribution of (a) thermal neutron flux in the core, measured in units of neutron/cm^2, and (b) temperature in the core, measured in units of Kelvin. $N_{\min}$ and $N_{\max}$ are the minimum and maximum neutron fluxes, respectively. $T_{\min}$ and $T_{\max}$ are the lowest and the highest temperatures, respectively.

4.3. The in-core burnup profile

We now examine the in-core burnup profile, by computing the time-averaged pebble burnup as a function of position. This provides insight into whether certain regions of the reactor (*e.g.* the central region, or the periphery) contain different amounts of pebble burnup. Here, we focus on the simplified case of pebble burnup during on a single drainage cycle, corresponding to always inserting fresh pebbles into the reactor; the more complex case of pebble recycling will be addressed in Sec. 5.

To generate the in-core burnup profile, we consider each of the pebbles in the trajectory database. Each trajectory consists of a number of time points and corresponding (r,z) position and burnup. Figures 14, 15, 16, & 17 show the spatial burnup distribution in the core for different values of μ_p and μ_w. As shown in Table 3 the gravity-driven flow rates vary considerably with friction, but here the simulation flow rate is scaled to match the real reactor flow rate. Hence the overall scale of burnup is similar for all cases.

Two competing effects govern the fine details of burnup. On the one hand, the neutron flux is highest in the center (Fig. 13(a)) and thus the central pebbles experience faster burnup. On the other hand, pebbles near the wall take longer to drain through the core (Fig. 12), and therefore experience slower burnup but for an increased duration. Taken together, these competing effects mean that the burnup distributions are somewhat uniform across the reactor for many of the combinations of μ_p and μ_w in Figs. 14–17. However, for cases with high μ_w where there is a strong boundary layer of slower flow, pebbles near the wall exhibit substantially higher burnup. By comparing to Fig. 7 we see that friction values with $R_v \lessapprox 0.75$ have a boundary layer of pebbles with enhanced burnup.

Figure 18 shows the statistical distribution of the burnup in the core when $\mu_w = 0.1$ and $\mu_w = 0.2$, based off all information in the pebble trajectory database. A bin size of 1.14 GWd/tU is used. Except for the last few bins in the tail of the distribution, the number of burnup values being analyzed in each bin is at the magnitude of 10^5–10^6, with the relative statistical error being as

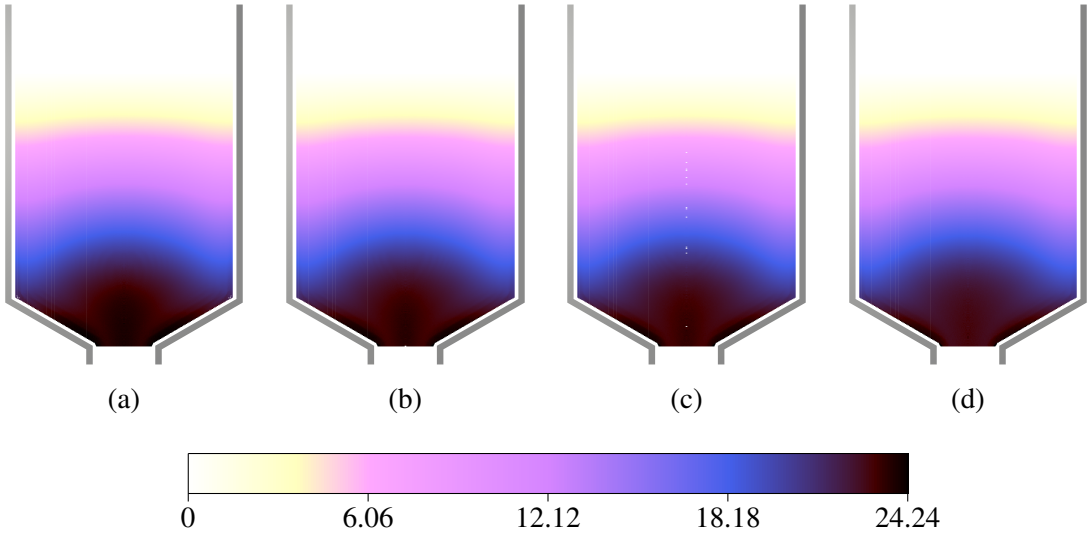

Figure 14: The spatial burnup distribution of the pebbles in the core undergoing one cycle, for $\mu_w = 0.1$ (in the unit of GWd/tU), varied with (a) $\mu_p = 0.05$, (b) $\mu_p = 0.125$, (c) $\mu_p = 0.2$ and (d) $\mu_p = 0.5$. Each pixel is colored based on the average burnup of pebbles located at that (r,z) location. If an (r,z) location has no data, it is colored white.

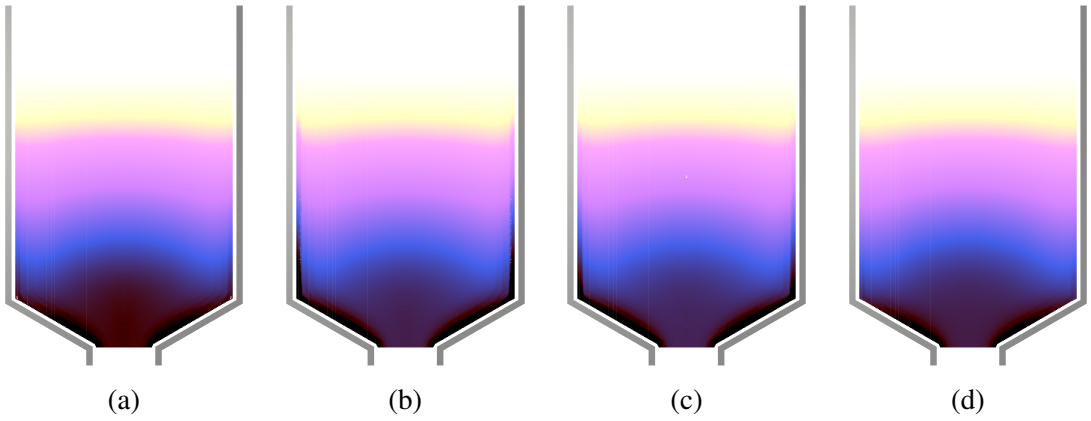

Figure 15: The spatial burnup distribution of the pebbles in the core undergoing one cycle, for $\mu_w = 0.2$, varied with (a) $\mu_p = 0.05$, (b) $\mu_p = 0.125$, (c) $\mu_p = 0.2$, and (d) $\mu_p = 0.5$. The color bar is the same as in Fig. 14.

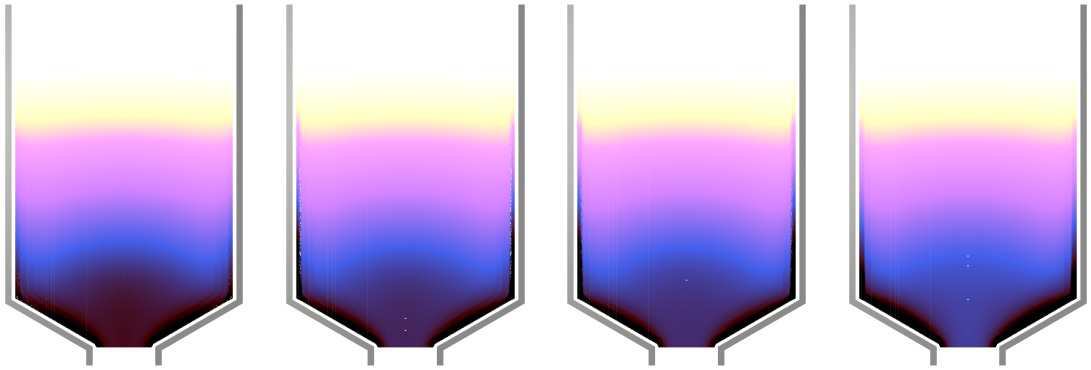

(a) (b) (c) (d)

Figure 16: The spatial burnup distribution of the pebbles in the core undergoing one cycle, for $\mu_w = 0.3$, varied with (a) $\mu_p = 0.05$, (b) $\mu_p = 0.125$, (c) $\mu_p = 0.2$, and (d) $\mu_p = 0.5$. The color bar is the same as in Fig. 14.

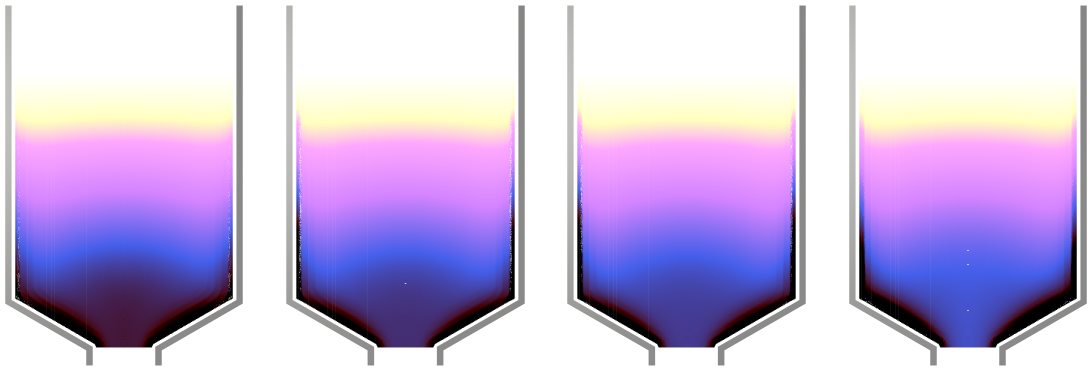

(a) (b) (c) (d)

Figure 17: The spatial burnup distribution of the pebbles in the core undergoing one cycle, for $\mu_w = 0.5$, varied with (a) $\mu_p = 0.05$, (b) $\mu_p = 0.125$, (c) $\mu_p = 0.2$, and (d) $\mu_p = 0.5$. The color bar is the same as in Fig. 14.

low as 0.1%. Hence, error bars are not shown for this plot or any similar one in the subsequent sections. Figure 18 shows two peaks at the front and end tail of the distribution. This is attributed to the neutron flux distribution in the core (Fig. 13(a)), which is much higher in the central height region and lower in the top and bottom region. Hence the pebble burnup increase per timestep as they pass through the top and bottom area is less than that in the central area, thus causing more intensive burnup in the initial and ending period of the distribution. For $\mu_w = 0.2$, the distributions for $\mu_p \in \{0.125, 0.2\}$ have an obvious tail due to the boundary pebbles.

4.4. The bottom burnup profile

4.4.1. Correlations with bottom burnup

We now examine the distribution of burnup in pebbles as they drain out of the reactor after completing one cycle. First, the relationship between the bottom burnup and some characteristic outputs is studied under the two friction cases of $\mu_w = 0.1$ and $\mu_w = 0.2$. The distribution for cases of $\mu_w = 0.3$ and $\mu_w = 0.5$ are similar to $\mu_w = 0.2$, and are not shown here.

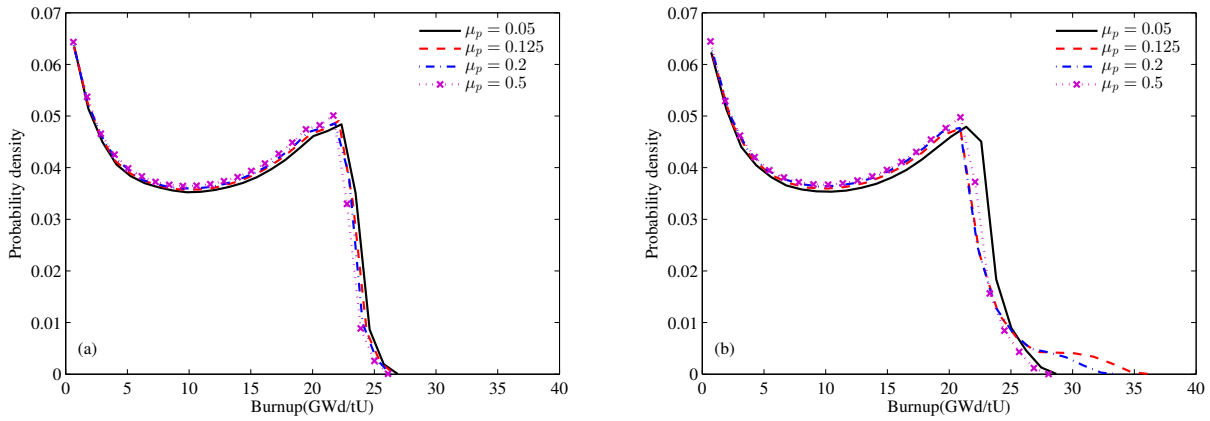

Figure 18: The probability density distribution of the burnup in the core of pebbles undergoing one cycle, with different μ_p under (a) $\mu_w = 0.1$ and (b) $\mu_w = 0.2$.

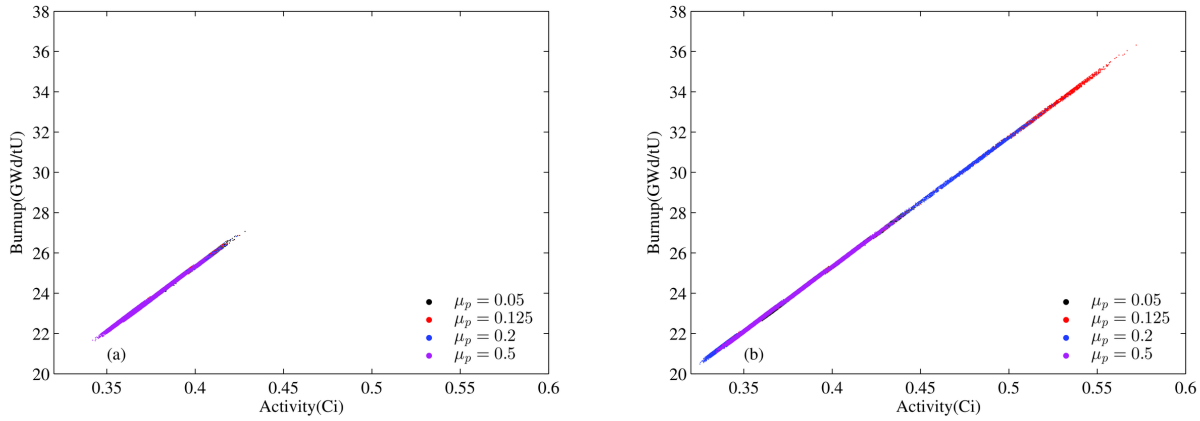

Figure 19: Correlations between the burnup and the activity of the Cs-137 at the bottom of the core for the pebbles undergoing one cycle, with different μ_p under (a) $\mu_w = 0.1$ and (b) $\mu_w = 0.2$.

Figure 19 shows a plot of the bottom burnup and the activity of Cs-137 of a pebble at the bottom for different values of μ_p. The relationship is almost linear, which is expected due to the high fission yield of CS-137, plus its low neutron-absorption cross-section and long half-life. When $\mu_w = 0.2$, the case with $\mu_p = 0.125$ has the most disperse distribution at the tail, where the most extreme boundary pebbles appear (Fig. 18(b)). For $\mu_w = 0.1$, there is no large difference between the different values of μ_p.

Figure 20 shows the relationship between the bottom burnup of a pebble and its initial radial position. Since the physical pebble flow rate is scaled to be equal, the mean burnup is similar in all cases, at approximately 23 GWd/tU. For cases with no boundary layer, the burnup profile is mainly uniform, but when a boundary layer is present ($\mu_w = 0.2$ & $\mu_p \in \{0.125, 0.2\}$) the burnup for pebbles near the wall is significantly larger. Furthermore, due to the layering of pebbles, the

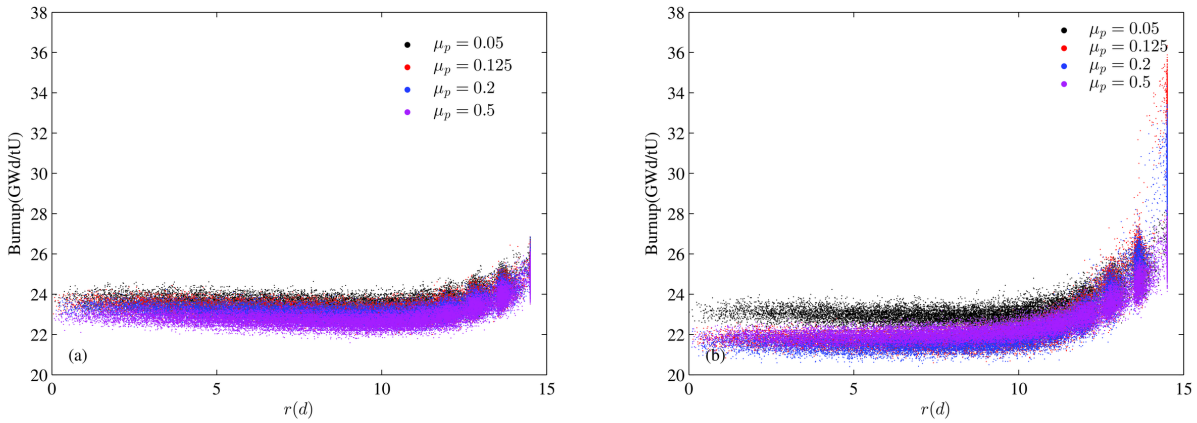

Figure 20: Correlations between the burnup at the bottom and the radial position at the top of the core for the pebbles undergoing one cycle, with different μ_p under (a) $\mu_w = 0.1$ and (b) $\mu_w = 0.2$.

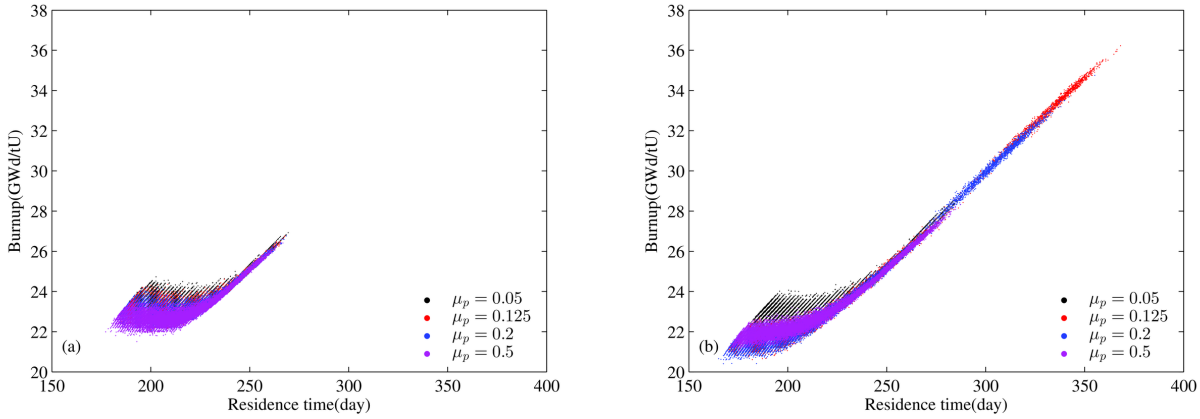

Figure 21: Correlations between the burnup at the bottom and the residence time from the top of the core for the pebbles undergoing one cycle, with different μ_p under (a) $\mu_w = 0.1$ and (b) $\mu_w = 0.2$.

pebbles that are next to the wall form a discrete population with higher burnup.

Figure 21 shows the relationship between bottom burnup and the residence time. For low residence times (200 d) there is some spread in the burnup. There is a range of pebble trajectories through the central region of the reactor that have similar residence times, but they experience different neutron fluxes, thus creating the burnup spread. On the contrary, for longer residence times there is a linear relationship between burnup and residence time, due to pebbles near the wall. All pebbles near the wall experience similar neutron fluxes, but as the previous analyses have shown, there can large variations in their residence time. This results in a one-to-one relationship between burnup and residence time.

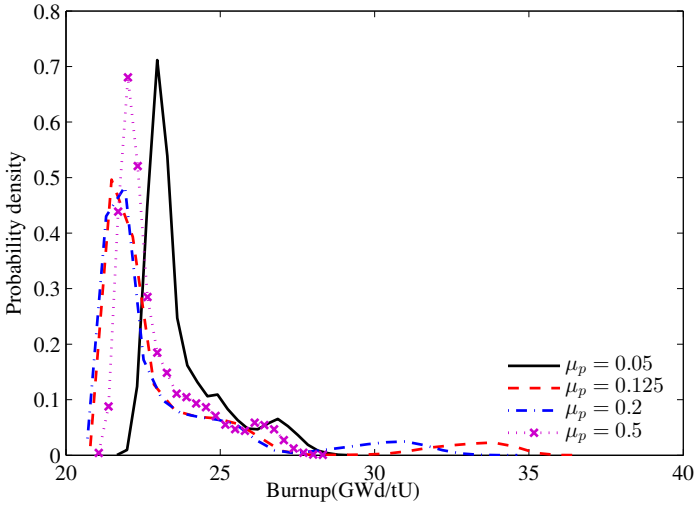

Figure 22: The one-cycle bottom burnup profile with different μ_p, and $\mu_w = 0.2$.

μ_p	0.05	0.125	0.2	0.5
Mean (GWd/tU)	23.76	23.34	23.08	22.94
St. Dev. (GWd/tU)	1.31	3.05	2.52	1.39

Table 4: The mean and standard deviation of the one-cycle bottom burnup distribution under different μ_p when $\mu_w = 0.2$.

4.4.2. Bottom burnup distribution

Figure 22 shows the bottom burnup distribution for $\mu_w = 0.2$ with different values of μ_p. There is a separate small peak in the tail of the distribution when $\mu_p \in \{0.125.0.2\}$, caused by the extreme burnup pebbles in the boundary region. The mean and standard deviation of the bottom burnup distribution for $\mu_w = 0.2$ are given in the Table 4. The mean value of burnup decreases slightly with μ_p, while the standard deviation is highest for the cases of $\mu_p \in \{0.125.0.2\}$ with the boundary layer. These statistical indicators are shown as a function of μ_p and μ_w in Fig. 23.

5. The construction of the multi-cycle pebble burnup profile

5.1. Introduction of the multi-cycle process

In the realistic PBR operation, each pebble will first drain slowly from the top through the core. The pebble burnup increases from B_0 to B after a cycle from top to the bottom, as shown by the pebble circulation model in Fig. 24. The pebble then drains outs of the exit pipe, where its burnup is measured to determine if it should be recycled back into the core or be discharged to a storage facility. Specifically, if the measured burnup B' exceeds a threshold B_d then the pebble is discharged; otherwise it is recycled. However, the burnup assay is not perfectly accurate, which can result in some *mis-recycled pebbles* that have $B > B_d$ and some *mis-discharged pebbles* that have $B \leq B_d$. In this section, we extend our analysis from Sec. 4 to examine the pebble burnup distributions over

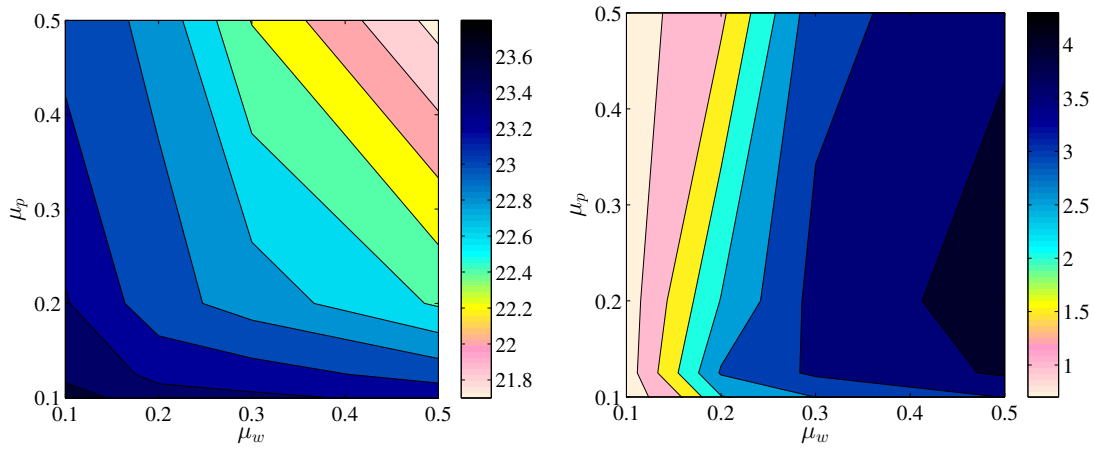

Figure 23: Color plots of (a) the mean and (b) the standard deviation for the one-cycle burnup distribution at the bottom of the core, measured in units of GWd/tU.

multiple drainage cycles. We examine the rates at which pebbles are recycled and discharged, and the fraction of mis-recycled and mis-discharged pebbles.

For a given pebble, our model of the burnup assay measurement B' is given by a Gaussian with probability density function

$$g(\xi) = \frac{1}{\sqrt{2\pi}\sigma_m(B)} e^{\frac{-[\xi-(1+s)B]^2}{2\sigma_m(B)^2}}, \tag{4}$$

where B is the real burnup of the pebble, and s is a systematic relative error. In real experimental measurements, the relative standard deviation has been shown to be a decreasing function of B (Yan et al., 2013). Following this previous study, we use a parabolic relation

$$\frac{\sigma_m(B)}{B} = aB^2 + bB + c \tag{5}$$

for some constants a, b, and c. In our analysis, if a pebble's true burnup is B, then we can simulate a burnup measurement B' by sampling a Gaussian random number with mean and standard deviation matching Eq. 4.

The aim of investigating the multi-cycle burnup profile is to study the burnup profile of the steady power stage of HTR-10 operation. To obtain a representative distribution of pebble burnup profiles in the steady power stage, we construct 100,000 multi-cycle pebble histories, with each history going from the time when the pebble is introduced to the time when it is discharged. We average the pebble burnup properties over this set of histories to obtain the pebble burnup profile under the steady operation.

The multi-cycle burnup calculation method is similar to the previous one-cycle method. To generate a multi-cycle pebble history, we randomly select a sequence of N one-cycle pebble

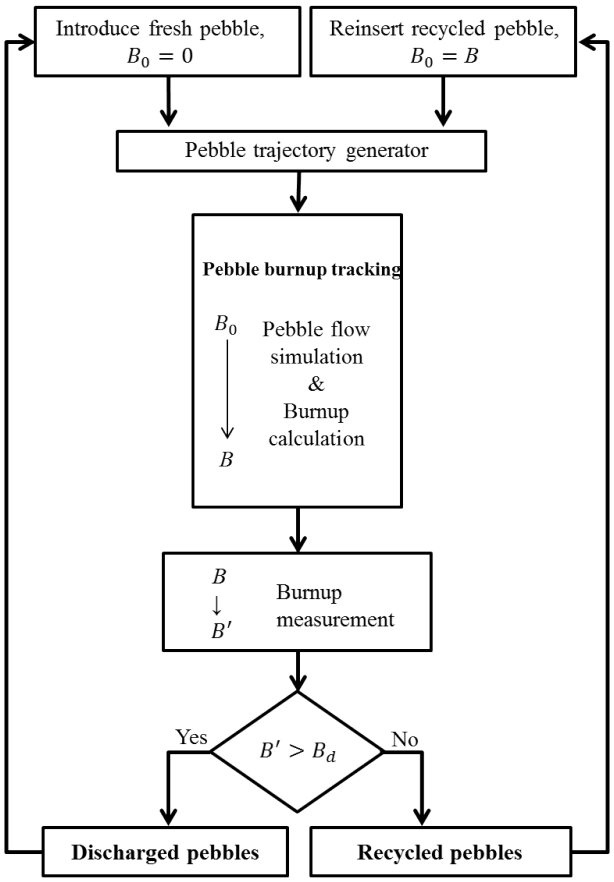

Figure 24: The model of pebble flow circulation in PBR.

trajectories. After that, the neutron flux and the temperature data along the multi-cycle trajectory of each pebble history is obtained. To match the real reactor operation, an $T_{\text{dec}} = 40$ d decay time between each cycle is also incorporated. Thereafter, KORIGEN input files for each multi-cycle pebble history is generated with all the data along trajectory prepared.

Once KORIGEN is run to calculate the burnup, each history is post-processed to determine when the pebble was discarded. After each cycle, a burnup measurement B' sampled according to Eq. 4, based on the true value of B. If $B' > B_d$ then the pebble is treated as discarded, and any further cycles in this multi-cycle history are ignored. Only the cycles before the discharge point are used in the subsequent analysis. In our study, we therefore choose N to be large enough that all pebbles have been discharged by the end of the multi-cycle history.

It should be noted that this procedure results a small loss in computational efficiency, since some burnup cycles calculated by KORIGEN are ignored. In principle, it would be more efficient to compute the burnup of each cycle in turn, and dynamically determine whether to continue depending on whether the burnup threshold has been reached. However, this would require modifications to the KORIGEN code itself, whereas here we use it as a black box. Furthermore, for the realistic HTR-10 parameters that we employ, there is limited variation in the number of cycles that each pebble passes through the reactor. We find that $N = 5$ is sufficient for all pebbles to be discharged.

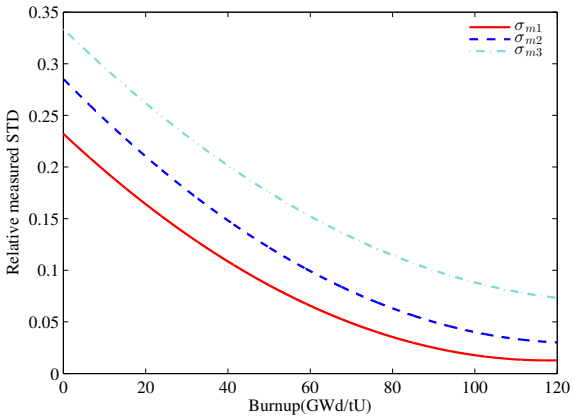

Figure 25: Plots of the three assumed functions, σ_{m1}, σ_{m2} and σ_{m3}, for the relative standard deviation (STD) of burnup measurement.

Since a typical pebble residence time for a single cycle is $T_{\text{typ. res.}} = 200$ d, the typical duration of a multi-cycle history is $NT_{\text{typ. res.}} + (N-1)T_{\text{dec}} \approx 1200$ d.

We choose parameters that are based upon reasonable estimates of HTR-10 operation. The measured burnup threshold $B_d = 72$ GWd/tU; the maximum allowable burnup in the core is $B_m = 100$ GWd/tU. The systematic error is assumed to be zero—while the realistic systematic error in non-zero, it can be partially corrected by calibration. Based on previous work (Yan et al., 2014), we consider three different functions $\sigma_{m1}(B)$, $\sigma_{m2}(B)$ and $\sigma_{m3}(B)$ with the form in Eq. 5 for the statistical error in measurement. The value of statistical error in the three curves at the burnup value point of 90 GWd/tU is 2.5%, 5% and 10%, respectively. Plots of these functions are given in Fig. 25, showing that the relative error decreases for higher values of burnup. These three error models will be compared in the subsequent analysis. Two groups of friction coefficients are chosen to compare the friction effects on the multi-cycle burnup profile: (a) $(\mu_w, \mu_p) = (0.3, 0.3)$, which has strong boundary layers, and (b) $(\mu_w, \mu_p) = (0.3, 0.05)$, which has no boundary layer.

5.2. The in-core burnup profile

Figure 26 shows the spatial burnup profile in the core under the two friction models, assuming zero burnup measuring error. Since the plot is based upon averaging pebbles that have undergone several different cycles there is more noise than in the corresponding single-cycle plots. The maximum spatially averaged burnup in the core is about 60 GWd/tU, and no area in the core is found to exceed B_m. The $\mu_p = 0.3$ case shows an obvious boundary layer which has higher burnup, while for $\mu_p = 0.05$ the high burnup area is evenly distributed in the conical region. These plots are similar to the single-cycle in-core burnup distributions.

Figure 27 shows the statistical distribution of the in-core burnup values. It shows several peaks and is fit using a Gaussian mixture model. Each peak corresponds to pebbles that have passed through the reactor for a different number of cycles. The general distributions for the two friction cases are similar, although the precise positioning of the peaks is different. Overall, the effects the measurement errors are small. However, for $\mu_p = 0.3$ and the largest error model σ_{m3}, a very small

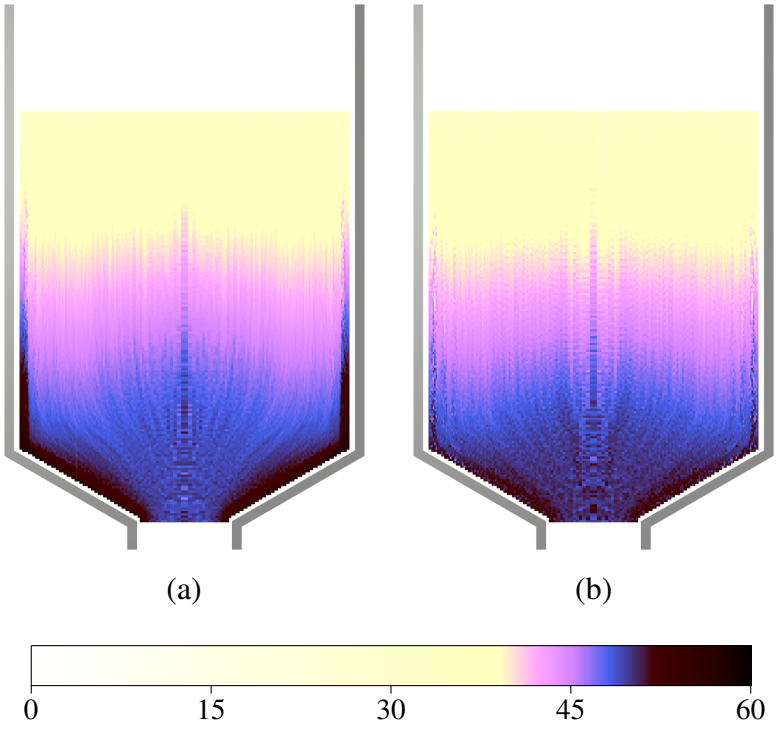

Figure 26: The spatial burnup distribution of the multi-cycle pebbles in the core for $\mu_w = 0.3$ (in units of GWd/tU), with (a) $\mu_p = 0.3$, (b) $\mu_p = 0.05$.

fraction of pebbles exceed the burnup threshold of $B_m = 100$ GWd/tU.

5.3. The bottom burnup profile

5.3.1. Correlations with bottom burnup

The relationship between the bottom burnup and the residence time is given in Fig. 28. The values are distributed into five groups for $\mu_p = 0.3$ corresponding to the maximum of five cycles that pebbles undergo. The first several groups are distinct, but become more dispersed and begin to overlap for more cycles. The points for the maximum measuring error, σ_{m3}, have the most disperse distribution. For $\mu_p = 0.05$, when the flow has no boundary layers, there is less dispersion in burnup during a single cycle, and consequently the five groups remain separate. Figure 29 shows the relationship between the bottom burnup and the activity of Cs-137, confirming that there is still a linear relationship between the two even after multiple cycles. The range of the Cs-137 activity in the distribution of $\mu_p = 0.3$ is 1.12–1.13 Ci as burnup reaches B_d (72 Gwd/tU). This provides a reference value for a Cs-137 measurement in the real burnup assay.

5.3.2. Bottom burnup distribution

Figure 30 shows the distribution of the bottom burnup. It also has several peaks, which are more pronounced than the in-core burnup distribution. The approximate average burnup of each cycle are at approximately 18 GWd/tU, 35 GWd/tU, 51 GWd/tU, 66 GWd/tU and 80 GWd/tU for $\mu_p = 0.3$.

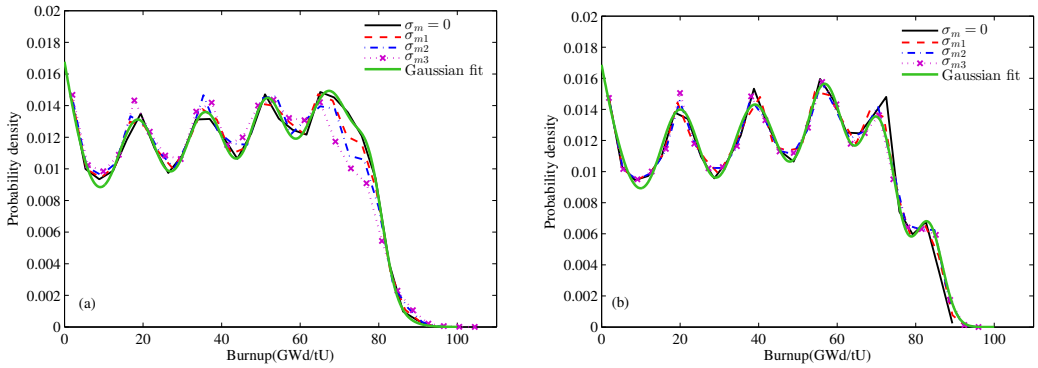

Figure 27: The probability density distribution of the burnup in the core for the multi-cycle pebbles with $\mu_w = 0.3$ and (a) $\mu_p = 0.3$ and (b) $\mu_p = 0.05$, under different burnup measuring accuracy.

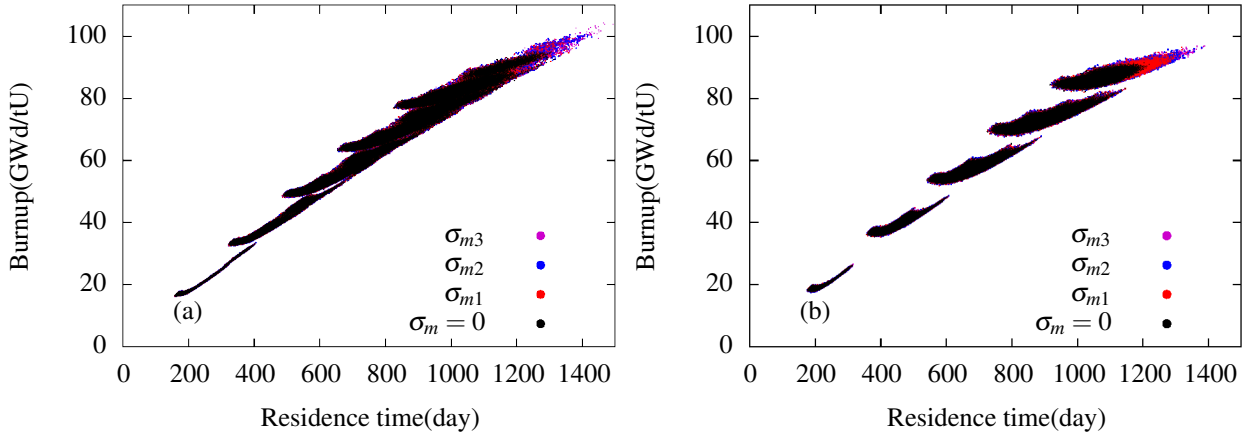

Figure 28: Correlations between the burnup and the residence time at the bottom of the core for the multi-cycle pebbles with $\mu_w = 0.3$ and (a)$\mu_p = 0.3$ and (b)$\mu_p = 0.05$, under different burnup measuring accuracy.

The tails of the distributions are more extended with a higher measuring error. For $\mu_p = 0.05$, the peaks in burnup are more distinct and are shifted to slightly higher values.

For the plots in Fig. 30, the distances between the peaks become progressively smaller for higher cycles. For example, for $\mu_p = 0.3$ the distance between peaks 1 and 2 is about 17 GWd/tU, whereas the distance between peaks 4 and 5 is about 14 GWd/tU. This indicates that the incremental burnup of each pebble decreases with the number of cycles, consistent with the nuclear fuel becoming progressively used. To obtain a clearer view of this phenomenon, Fig. 31 gives the distributions of incremental burnups for pebbles on different numbers of cycles, showing that the peaks move leftward as the number of cycles increases. The plot shows the distributions for both zero measuring error, and the maximum measuring error model σ_{m3}. For the first four cycles, there is a negligible difference between the two error models—this should be expected, since at the point when these pebbles are recycled, their burnup values will be well below the threshold B_d. For the fifth cycle when $\mu_p = 0.3$, a minor difference in the peak is visible—this observation will be returned to later.

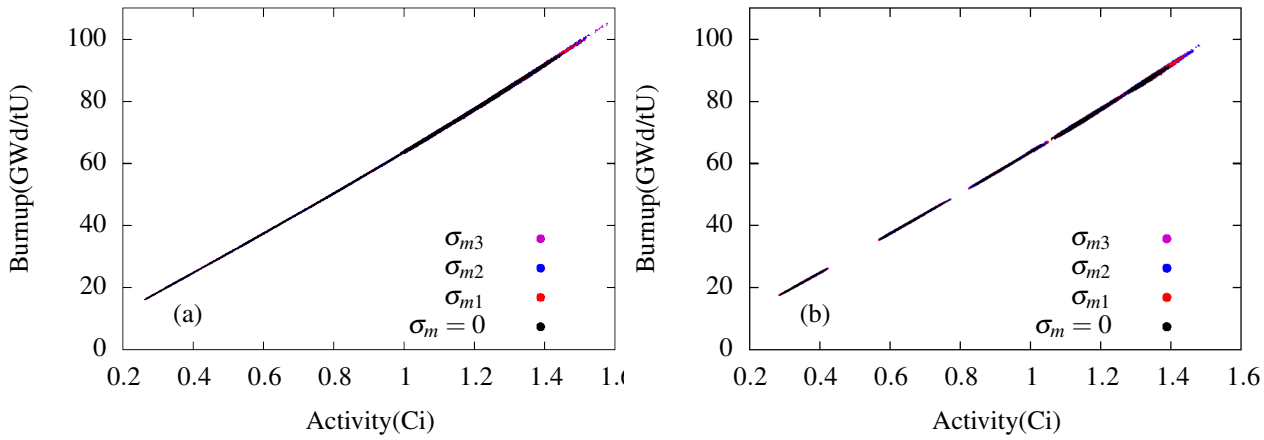

Figure 29: Correlations between the burnup and the activity of the Cs-137 at the bottom of the core for the multi-cycle pebbles with $\mu_w = 0.3$ and (a) $\mu_p = 0.3$ and (b) $\mu_p = 0.05$, under different burnup measuring accuracy.

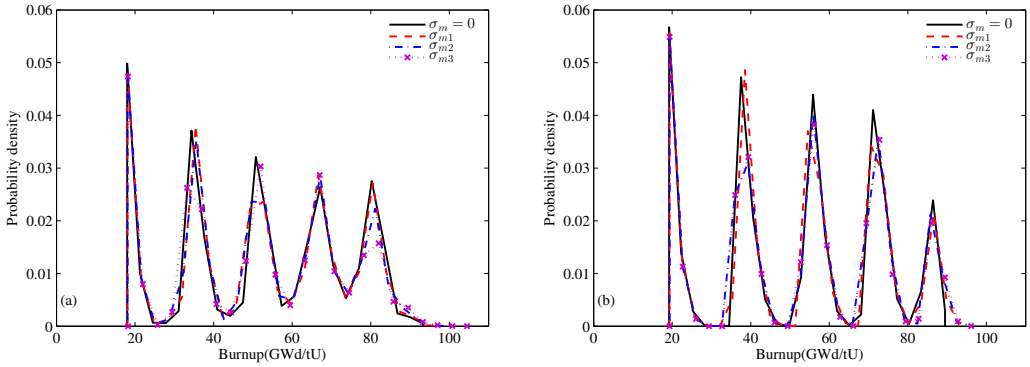

Figure 30: The probability density distribution of the burnup at the bottom of the core for the multi-cycle pebbles with $\mu_w = 0.3$ and (a) $\mu_p = 0.3$ and (b) $\mu_p = 0.05$, under different burnup measuring accuracy.

Both graphs show long tails and additional small peaks in the distributions due to the boundary pebbles. As expected, these peaks are stronger for $\mu_p = 0.3$, which has the strong boundary layers.

Figures 32 & 33 show the burnup distributions of discharged and recycled pebbles, respectively. Different behavior is seen for the two different values of pebble–pebble friction, due to the positioning of the burnup threshold $B_d = 72$ GWd/tU. Examining Fig. 30 shows that for $\mu_p = 0.3$, the burnup threshold appears after the peak for the fourth cycle, and therefore most pebbles will be discharged after their fifth cycle. However, for $\mu_p = 0.05$, the burnup threshold closely matches the peak of the fourth cycle, so pebbles will be discharged after four and five cycles with roughly equal probability. This behavior can be seen in Fig. 32, whereby the $\mu_p = 0.05$ case has two peaks, while the $\mu_p = 0.3$ has one large peak. In real reactor operation, it may be preferable to tune the burnup threshold to lie between peaks, since this will mean that the majority of pebbles will be discharged after the same number of cycles.

For $\mu_p = 0.3$, measurement error can substantially affect the discharge burnup distribution. For

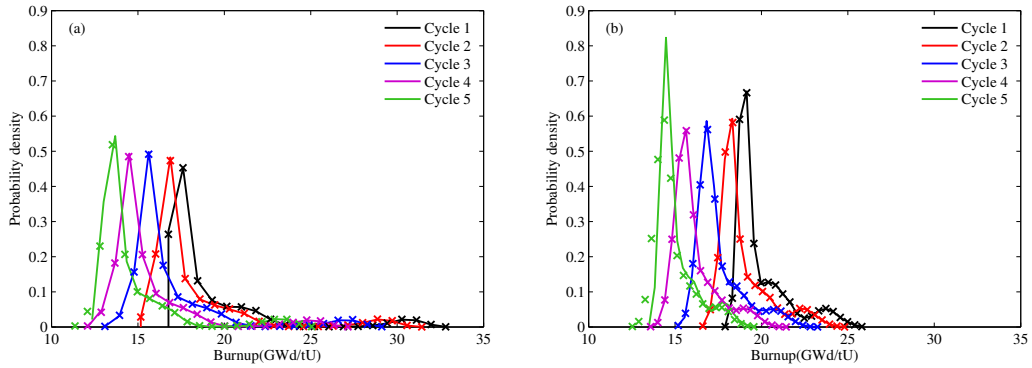

Figure 31: The probability density distribution of the burnup increase of each cycle for the multi-cycle pebbles with $\mu_w = 0.3$ and (a) $\mu_p = 0.3$ and (b) $\mu_p = 0.05$, without measuring error (solid line) and with measuring error σ_{m3} (x-point line).

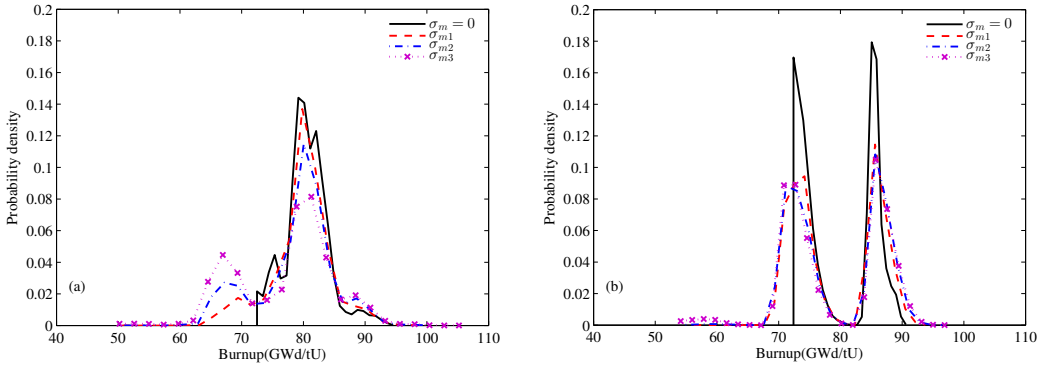

Figure 32: The probability density distribution of the burnup for the discharged pebbles at the bottom with $\mu_w = 0.3$ and (a) $\mu_p = 0.3$ and (b) $\mu_p = 0.05$, under different burnup measuring accuracy.

the σ_{m2} and σ_{m3} models, a second peak is visible in Fig. 32(a), corresponding to mis-discharged pebbles; it is likely that many of these pebbles were discharged after four cycles instead of five. Since the burnup composition of the discharged pebbles is different for the σ_{m3} model, this may explain why the five-cycle plot in Fig. 31 is slightly different in this case.

5.4. Statistics on the proportions of discharged and recycled pebbles

For the two different friction parameter sets that we consider, we now now examine quantitatively the proportions of pebbles that are discharged and recycled. Tables 5 & 6 both give the discharged proportion P_{dis} and the recycled proportion P_{rec}. The tables also lists the mis-discharged proportion P_{mdis}, defined as the proportion of mis-discharged pebbles in all of the discharged pebbles. Similarly, the table lists the mis-recycled pebbles, defined as the proportion of mis-recycled pebbles in all of the recycled pebbles. Finally, the table lists the proportion P_{max} of all pebbles the exceed the maximum allowable burnup B_m.

The tables reveal that the discharged proportion increases with the measuring error, and the value

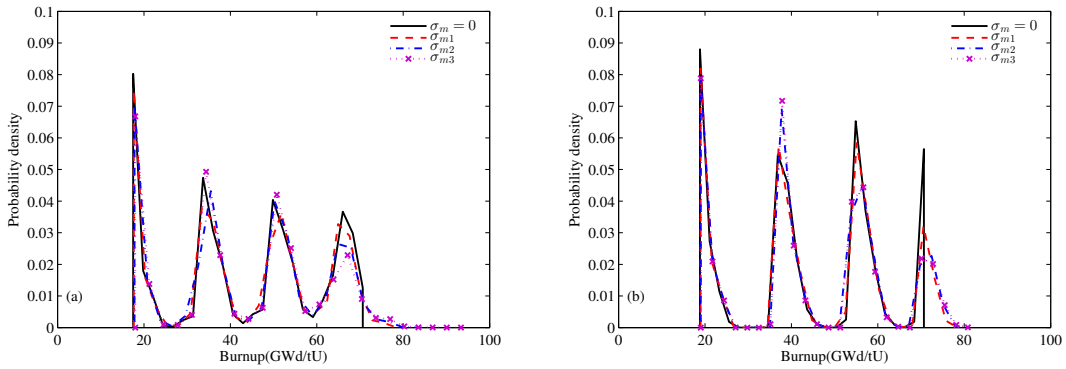

Figure 33: The probability density distribution of the burnup for the recycled pebbles at the bottom with $\mu_w = 0.3$ and (a) $\mu_p = 0.3$ and (b) $\mu_p = 0.05$, under different burnup measuring accuracy.

	$\sigma_m = 0$	σ_{m1}	σ_{m2}	σ_{m3}
P_{dis}	20.96%	21.23%	21.56%	22.05%
P_{rec}	79.04%	78.77%	78.44%	77.95%
P_{mdis}	0	9.32%	18.09%	29.40%
P_{mrec}	0	0.87%	1.46%	2.13%
P_{max}	0	0	2.39×10^{-6}	1.49×10^{-5}

Table 5: Proportions of pebbles that are discharged (P_{dis}), recycled (P_{rec}), mis-discharged (P_{mdis}), mis-recycled (P_{mrec}), and exceed the maximum burnup threshold (P_{max}) in the multi-cycle analysis with $\mu_p = 0.3$ and $\mu_w = 0.3$. See the main text for precise definitions of these proportions. Data for zero measuring error ($\sigma_m = 0$) and for the three measuring error models σ_{m1}, σ_{m2}, and σ_{m3} are shown.

	$\sigma_m = 0$	σ_{m1}	σ_{m2}	σ_{m3}
P_{dis}	22.45%	22.47%	22.43%	22.56%
P_{rec}	77.55%	77.53%	77.57%	77.44%
P_{mdis}	0	16.29%	19.23%	23.36%
P_{mrec}	0	4.61%	5.73%	6.48%
P_{max}	0	0	0	0

Table 6: Proportions of pebbles that are discharged (P_{dis}), recycled (P_{rec}), mis-discharged (P_{mdis}), mis-recycled (P_{mrec}), and exceed the maximum burnup threshold (P_{max}) in the multi-cycle analysis with $\mu_p = 0.05$ and $\mu_w = 0.3$. See the main text for precise definitions of these proportions. Data for zero measuring error ($\sigma_m = 0$) and for the three measuring error models σ_{m1}, σ_{m2}, and σ_{m3} are shown.

is around 20%–22%, which is consistent with the number of the cycles. The tables also suggest that the average number of cycles is sensitive to the assay accuracy and the friction coefficients. For the case without measuring error, the mis-discharged, mis-recycled and the $P_{\max}$ proportion are all zero, whereas they begin to increase with increasing measuring error. However, the mis-discharged proportion is much higher than the mis-recycled proportion. This is likely due to two reasons. First, the total number of recycled pebbles is larger. Second, the precise positioning of B_d in relation to the bottom burnup distribution plays a role (as discussed in Subsec. 5.3.2), since there are substantially more pebbles with burnups that are slightly below B_d than slightly above B_d. For large measurement error, a very small proportion of pebbles exceed the maximum allowable burnup.

Tables 5 & 6 are generally quite similar. However in Table 6, the $P_{\max}$ value is zero for all the measuring accuracy models, even though there are still mis-recycled pebbles in the core. Since the case with $\mu_p = 0.05$ does not have strong boundary layers, the spread in burnup during on cycle is lower, and so even if a pebble is mis-recycled, it will still remain within the burnup limit of (100 GWd/tU) after another cycle of irradiation in the code. Although the $P_{\max}$ values for $\mu_p = 0.05$ are zero, its mis-discharge proportion is higher than that for $\mu_p = 0.3$. This results shows that having limited or no velocity boundary layers may be beneficial, since the pebble burnup increases have a lower spread, making it easier to carefully control the burnup distributions.

The effects of systematic error on the proportion data are presented in Tables 7 & 8. Results for five systematic errors s ranging from -2% to 2% are compared. Table 7 shows that the P_{dis} and P_{mdis} increase with the increasing systematic error, whereas the P_{rec}, P_{mrec} and $P_{\max}$ decrease with increasing systematic error. This should be expected, since a positive systematic error will increase the average value of B' and therefore increase the likelihood of a pebble being discharged. A positive systematic error would therefore result in a loss of reactor efficiency, since more pebbles will be discharged before reaching the desired burnup level. For $\mu_p = 0.3$, the highest value of $P_{\max}$ occurs with a systematic error of -2% and the large measuring error model, σ_{m3}. However, even in this case the proportion of pebbles exceeding B_m is still only 0.00170%. For $\mu_p = 0.05$, no pebbles exceeding B_m are found under any of the error models considered.

6. Conclusion

This paper introduces an approach for calculating the burnup of individual pebbles to construct the burnup profile of fuel pebbles in a PBR. The method combines pebble flow simulation and the burnup calculation. By computing the burnup of each pebble individually, the approach has a major advantage of being able to accurately quantify extremal statistics of pebble burnup, which may have important consequences for reactor safety. Our results show that the extremal statistics of pebble burnup are strongly influenced by the presence of boundary layers of slower pebble flow near the reactor walls. In both our single-cycle and multi-cycle analyses, pebble flows with strong boundary layers had larger tails in the burnup profile, which in certain regimes can result in a small fraction of pebbles exceeding a maximum allowable burnup threshold B_m.

Given the importance of the boundary layers, we performed a comprehensive study of the effect of pebble–pebble friction μ_p and pebble–wall friction μ_w on the pebble flow profile. Our results show that the strength of the boundary layers is a surprisingly complex function of the friction parameters. In particular, for certain values of μ_w, the boundary layer strength depends

		$s=-2\%$	$s=-1\%$	$s=-0\%$	$s=+1\%$	$s=+2\%$
	P_{dis}	20.94%	21.08%	21.23%	21.41%	21.60%
	P_{rec}	79.06%	78.92%	78.77%	78.59%	78.40%
σ_{m1}	P_{mdis}	5.12%	6.99%	9.32%	12.34%	15.69%
	P_{mrec}	1.51%	1.15%	0.87%	0.66%	0.45%
	P_{max}	3.38×10^{-7}	1.17×10^{-7}	0	0	0
	P_{dis}	21.27%	21.40%	21.56%	21.71%	21.90%
	P_{rec}	78.73%	78.60%	78.44%	78.29%	78.10%
σ_{m2}	P_{mdis}	13.56%	15.63%	18.09%	20.56%	23.78%
	P_{mrec}	2.00%	1.73%	1.46%	1.23%	1.03%
	P_{max}	2.35×10^{-6}	4.72×10^{-7}	2.39×10^{-6}	3.65×10^{-7}	0
	P_{dis}	21.84%	21.94%	22.05%	22.18%	22.29%
	P_{rec}	78.16%	78.06%	77.95%	77.82%	77.71%
σ_{m3}	P_{mdis}	26.18%	27.74%	29.40%	31.35%	33.10%
	P_{mrec}	2.51%	2.32%	2.13%	1.94%	1.78%
	P_{max}	1.70×10^{-5}	1.61×10^{-5}	1.49×10^{-5}	8.45×10^{-6}	7.76×10^{-6}

Table 7: Proportions of pebbles that are discharged (P_{dis}), recycled (P_{rec}), mis-discharged (P_{mdis}), mis-recycled (P_{mrec}), and exceed the maximum burnup threshold (P_{max}) in the multi-cycle analysis with $\mu_p = 0.3$ and $\mu_w = 0.3$, using different values of systematic error s in the burnup assay. See the main text for precise definitions of these proportions.

		$s=-2\%$	$s=-1\%$	$s=-0\%$	$s=+1\%$	$s=+2\%$
	P_{dis}	21.76%	22.11%	22.47%	22.85%	23.22%
	P_{rec}	78.24%	77.89%	77.53%	77.15%	76.78%
σ_{m1}	P_{mdis}	10.12%	13.19%	16.29%	20.07%	23.81%
	P_{mrec}	6.77%	5.68%	4.61%	3.67%	2.76%
	P_{max}	0	0	0	0	0
	P_{dis}	21.93%	22.16%	22.43%	22.66%	22.94%
	P_{rec}	78.07%	77.84%	77.57%	77.34%	77.06%
σ_{m2}	P_{mdis}	14.71%	16.73%	19.23%	21.42%	23.93%
	P_{mrec}	7.14%	6.43%	5.73%	5.08%	4.35%
	P_{max}	0	0	0	0	0
	P_{dis}	22.26%	22.40%	22.56%	22.71%	22.88%
	P_{rec}	77.74%	77.60%	77.44%	77.29%	77.12%
σ_{m3}	P_{mdis}	20.54%	21.88%	23.36%	24.88%	26.44%
	P_{mrec}	7.25%	6.88%	6.48%	6.11%	5.72%
	P_{max}	0	0	0	0	0

Table 8: Proportions of pebbles that are discharged (P_{dis}), recycled (P_{rec}), mis-discharged (P_{mdis}), mis-recycled (P_{mrec}), and exceed the maximum burnup threshold (P_{max}) in the multi-cycle analysis with $\mu_p = 0.05$ and $\mu_w = 0.3$, using different values of systematic error s in the burnup assay. See the main text for precise definitions of these proportions.

non-monotonically on μ_p, which can be explained by examining whether pebbles can spin, and slide on pebble–pebble contacts. A wide range of friction coefficients for graphite that have been reported in the literature (Luo et al., 2010), and there are additional uncertainties that are introduced by the extreme operating environment in a PBR core. We note that the friction values over which we observe the complex non-monotonic boundary layer behavior are within the realms of feasibility for friction values in a real reactor. Relatively small changes in friction coefficients can have a large effect on the boundary layer behavior, and therefore may be an important design consideration.

Our burnup analysis is based on first constructing a database of representative pebble trajectories through the core, which are taken from DEM simulation. Once the database is assembled, it can be analyzed for relatively low computational cost, without having to re-run the DEM simulation. We first analyzed the pebble burnup over a single drainage cycle. Our results showed that the stronger the flow boundary layers, the larger the variation in burnup. Furthermore, there is a close relationship between burnup and residence time in the reactor, which could be a useful design consideration. For example, previous work has shown that altering the angle of the funnel region strongly affects the residence time distribution Rycroft et al. (2006b), and thus it is likely that this would affect the burnup distribution as well. In addition, our results show that the amount of burnup a pebble experiences are strongly influenced by its initial radial position. This suggests another interesting design possibility, whereby pebbles close to the burnup threshold B_d could be inserted near $r = 0$, since those pebbles tend to experience the lowest amount of burnup with the lowest amount of variation; hence, these pebbles would be unlikely to exceed the maximum allowable threshold B_m. By contrast, fresh pebbles could be inserted near the reactor vessel wall, since they can tolerate being irradiated to a larger degree.

In addition, we also considered a full multi-cycle analysis of the burnup profile, incorporating the burnup assay to determine whether pebbles are recycled or discharged, which is a more realistic model of the steady power stage of the HTR-10. We examined the increase in pebble burnup over one cycle, and the number of mis-recycled and mis-discharged pebbles. For the realistic parameters that we used, the variations in pebble burnup were small in comparison to the mean pebble burnup. This meant that the distributions of pebble burnup at the bottom of the reactor could be clearly distinguished into a number of separate peaks, each corresponding to pebbles undergoing a different number of cycles. Consequently, it may be worth tuning the bottom burnup threshold B_d to lie between these peaks, so that the vast majority of pebbles are discharged after a certain chosen number of cycles. For two different friction cases, we reported detailed statistics on the proportions of pebbles that are discharged and recycled. We examined how the burnup assay affects these proportions, considering both systematic error and random error. For the realistic parameters that we chose, even with a large amount of burnup assay error, we found that only a minuscule proportion of pebbles would exceed the maximum allowable pebble burnup.

In this paper, our primary aim has been to develop and test the computational analysis approach, and therefore in our multi-cycle study, we focused on the simplified case where the neutron flux and reactor temperature are assumed to be constant in time. However, in realistic HTR-10 operation, the neutron flux in the core changes with the running time. Our computational approach can easily be adapted to calculate burnup distributions for the case of a non-steady neutron flux, and since it can be run relatively inexpensively without requiring DEM simulation, it is fast enough for real-time

analysis. Moreover, the computational approach will be applied to study the burnup profile in HTR-PM geometry, to provide information for the future operation and burnup assay of HTR-PM.

Acknowledgments

This project is supported by the National Science and Technology Major Project [grant number ZX06901] and the Nuclear Energy Development Project jointly. Y. Tang was supported by the China Scholarship Council. C. H. Rycroft was partially supported by the Director, Office of Science, Computational and Technology Research, U. S. Department of Energy under Contract No. DE-AC02-05CH11231.

Bibliography

Adamantiades, A., Kessides, I., 2009. Nuclear power for sustainable development: current status and future prospects. Energy Policy 37, 5149–5166.

Aranson, I.S., Tsimring, L.S., 2002. Continuum theory of partially fluidized granular flows. Phys. Rev. E 65, 061303.

Bazant, M.Z., 2006. The spot model for random-packing dynamics. Mechanics of Materials 38, 717–731.

Caram, H., Hong, D.C., 1991. Random-walk approach to granular flows. Phys. Rev. Lett. 67, 828–831.

Chen, H., Fu, L., 2014. Investigation on the pebble bed flow model in VSOP. Nuclear Engineering and Design 271, 352–355.

Choi, J., Kudrolli, A., Rosales, R.R., Bazant, M.Z., 2004. Diffusion and mixing in gravity-driven dense granular flows. Phys. Rev. Lett. 92, 174301.

Christoffersen, J., Mehrabadi, M.M., Nemat-Nasser, S., 1981. A micromechanical description of granular material behavior. Journal of Applied Mechanics 48, 339–344.

Cogliati, J.J., Ougouag, A.M., 2006. PEBBLES: A computer code for modeling packing, flow and re-circulation of pebbles in a pebble bed reactor, in: 3rd International Topical Meeting on High Temperature Reactor Technology, Johannesburg, South Africa.

Cogliati, J.J., Ougouag, A.M., 2008. Pebble bed reactor dust production model, in: Proceedings of the 4th International Topical Meeting on High Temperature Reactor Technology.

Cundall, P.A., Strack, O.D.L., 1979. A discrete numerical model for granular assemblies. Géotechnique 29, 47–65.

Depken, M., Lechman, J.B., van Hecke, M., van Saarloos, W., Grest, G.S., 2007. Stresses in smooth flows of dense granular media. Europhys. Lett. 78, 58001.

Dunatunga, S., Kamrin, K., 2015. Continuum modelling and simulation of granular flows through their many phases. Journal of Fluid Mechanics 779, 483–513.

Fischer, U., Wiese, H.W., 1983. Verbesserte konsistente Berechnung des nuklearen Inventars abgebrannter DWR-Brennstoffe auf der Basis von Zell-Abbrand-Verfahren mit KORIGEN. Kernforschungszentrum Karlsruhe.

Gottaut, H., Krüger, K., 1990. Results of experiments at the AVR reactor. Nuclear Engineering and Design 121, 143–153.

Gougar, H.D., 2004. Advanced Core Design and Fuel Management for Pebble-Bed Reactors. Ph.D. thesis. Pennsylvania State University.

Guo, X., Guo, X., 2016. Nuclear power development in China after the restart of new nuclear construction and approval: A system dynamics analysis. Renewable and Sustainable Energy Reviews 57, 999–1007.

Hassan, Y.A., 2008. Large eddy simulation in pebble bed gas cooled core reactors. Nuclear Engineering and Design 238, 530–537.

Henann, D.L., Kamrin, K., 2013. A predictive, size-dependent continuum model for dense granular flows. Proceedings of the National Academy of Sciences 110, 6730–6735.

IAEA-TECDOC-1198, 2001. Current status and future development of modular high temperature gas cooled reactor technology. Technical Report IAEA-TECDOC-1198. International Atomic Energy Agency.

IAEA-TECDOC-1382, 2003. Evaluation of High Temperature Gas Cooled Reactor performance: benchmark analysis related to initial testing of the HTTR and HTR-10. Technical Report IAEA-TECDOC-1382. International Atomic Energy Agency.

IAEA-TECDOC-1674, 2012. Advances in HTGR fuel technology. Technical Report IAEA-TECDOC-1674. International Atomic Energy Agency.

IEA, 2017. International energy agency, key world energy statistics. https://www.iea.org/publications/freepublications/publication/KeyWorld2017.pdf.

Ion, S., Nicholls, D., Matzie, R., Matzner, D., 2004. Pebble bed modular reactor—the first generation IV reactor to be constructed. Nuclear Energy 43, 55–62.

Jaeger, H.M., Nagel, S.R., Behringer, R.P., 1996. Granular solids, liquids, and gases. Rev. Mod. Phys. 68, 1259–1273.

Janssen, H.A., 1895. Versuche über getreidedruck in silozellen. Zeitschr. d. Vereines deutscher Ingenieure 39, 1045.

Jiang, S., Yang, X., Tang, Z., Wang, W., Tu, J., Liu, Z., Li, J., 2012. Experimental and numerical validation of a two-region-designed pebble bed reactor with dynamic core. Nuclear Engineering and Design 246, 277–285.

Jiang, Y., Liu, M., 2003. Granular elasticity without the Coulomb condition. Phys. Rev. Lett. 91, 144301.

Jop, P., Forterre, Y., Pouliquen, O., 2006. A constitutive law for dense granular flows. Nature 441, 727–730.

Kadanoff, L.P., 1999. Built upon sand: Theoretical ideas inspired by granular flows. Rev. Mod. Phys. 71, 435–444.

Kamrin, K., Rycroft, C.H., Bazant, M.Z., 2007. The stochastic flow rule: A multi-scale model for granular plasticity. Modelling Simul. Mater. Sci. Eng. 15, S449–S464.

Kim, H.C., Kim, S.H., Kim, J.K., Noh, J.M., 2008. Monte Carlo burn-up calculation for 400 MW_{th} PBMR startup core .

Kissane, M., 2009. A review of radionuclide behaviour in the primary system of a very-high-temperature reactor. Nuclear Engineering and Design 239, 3076–3091.

Koster, A., Matzner, H., Nicholsi, D., 2003. Pbmr design for the future. Nuclear Engineering and Design 222, 231–245.

LAMMPS website, . http://lammps.sandia.gov/. [Online; accessed June 21st, 2013].

Landry, J.W., Grest, G.S., Plimpton, S.J., 2004. Discrete element simulations of stress distributions in silos: crossover from two to three dimensions. Powder Technology 139, 233–239.

Landry, J.W., Grest, G.S., Silbert, L.E., Plimpton, S.J., 2003. Confined granular packings: Structure, stress, and forces. Phys. Rev. E 67, 041303.

Lind, T., Güntay, S., Dehbi, A., Liao, Y., Rycroft, C.H., 2010. PSI project on HTR dust generation and transport, in: Proceedings of HTR 2010.

Litwiniszyn, J., 1963. The model of a random walk of particles adapted to researches on problems of mechanics of loose media. Bull. Acad. Pol. Sci. 11, 593.

Locatelli, G., Mancini, M., Todeschini, N., 2013. Generation IV nuclear reactors: Current status and future prospects. Energy Policy 61, 1503–1520.

Luo, X., Li, X., Yu, S., 2010. Nuclear graphite friction properties and the influence of friction properties on the pebble bed. Nuclear Engineering and Design 240, 2674–2681.

Majmudar, T.S., Behringer, R.P., 2005. Contact force measurements and stress-induced anisotropy in granular materials. Nature 435, 1079–1082.

Matsson, I., 1995. ORIGEN2 simulations of spent BWR fuel with different burnup, power history and initial enrichment. SKI Report 95, 46.

Mueth, D.M., Jaeger, H.M., Nagel, S.R., 1998. Force distribution in a granular medium. Phys. Rev. E 57, 3164–3169.

Mullins, W., 1974. Experimental evidence for the stochastic theory of particle flow under gravity. Powder Technology 9, 29–37.

Mullins, W.W., 1972. Stochastic theory of particle flow under gravity. Journal of Applied Physics 43, 665–678.

NEI News, 2017. Milestones. https://www.nei.org/News-Media/News/Milestones.

Oppe, J., Kuijper, J.C., de Haas, J.B.M., Verkerk, E.C., Klippel, H.T., 2001. Modeling of continuous reload HTR systems by the PANTHERMIX code system, in: Transactions of the American Nuclear Society Topical Meeting on Mathematics and Computation, Salt Lake City, Utah.

Ougouag, A.M., Cogliati, J.J., Kloosterman, J.L., 2005. Methods for modeling the packing of fuel elements in pebble-bed reactors, in: Proceedings of the Topical Meeting on Mathematics and Computation, Avignon, France, American Nuclear Society, LaGrange Park, IL.

Plimpton, S.J., 1995. Fast parallel algorithms for short-range molecular dynamics. J. Comput. Phys. 117, 1–19.

Pöschel, T., Schwager, T., 2005. Computational Granular Dynamics: Models and Algorithms. Springer.

Rycroft, C.H., Bazant, M.Z., Grest, G.S., Landry, J.W., 2006a. Dynamics of random packings in granular flow. Phys. Rev. E 73, 051306.

Rycroft, C.H., Dehbi, A., Lind, T., Güntay, S., 2012a. Granular flow in pebble-bed nuclear reactors: Scaling, dust generation, and stress. Nuclear Engineering and Design 265, 69–84.

Rycroft, C.H., Grest, G.S., Landry, J.W., Bazant, M.Z., 2006b. Analysis of granular flow in a pebble-bed nuclear reactor. Phys. Rev. E 74, 021306.

Rycroft, C.H., Lind, T., Güntay, S., Dehbi, A., 2012b. Granular flow in pebble-bed reactors: scaling and dust generation, in: Proceedings of ICAPP 2012, American Nuclear Society, Chicago.

Rycroft, C.H., Orpe, A.V., Kudrolli, A., 2009. Physical test of a particle simulation model in a sheared granular system. Phys. Rev. E 80, 031305.

Rycroft, C.H., Wong, Y.L., Bazant, M.Z., 2010. Fast spot-based multiscale simulations of granular drainage. Powder Technology 200, 1–11.

Silbert, L.E., Ertaş, D., Grest, G.S., Halsey, T.C., Levine, D., 2002. Geometry of frictionless and frictional sphere packings. Phys. Rev. E 65, 031304.

Silbert, L.E., Ertaş, D., Grest, G.S., Halsey, T.C., Levine, D., Plimpton, S.J., 2001. Granular flow down an inclined plane: Bagnold scaling and rheology. Phys. Rev. E 64, 051302.

Sperl, M., 2006. Experiments on corn pressure in silo cells – translation and comment of Janssen's paper from 1895. Granular Matter 8, 59–65.

Stempniewicz, M., Winters, L., Caspersson, S., 2012. Analysis of dust and fission products in a pebble bed ngnp. Nuclear Engineering and Design 251, 433–442. 5th International Topical Meeting on High Temperature Reactor Technology (HTR 2010).

Tang, Y., Zhang, L., Guo, Q., Cao, J., Tong, J., 2016. A proposed model to describe the relationship between online burnup assay and economy and safety of pebble bed reactor, in: 2016 24th International Conference on Nuclear Engineering, American Society of Mechanical Engineers. p. V001T02A012.

du Toit, C., 2002. The numerical determination of the variation in the porosity of pebble-bed core, in: Proceedings of the Conference on High-Temperature Reactors, Petten, NL, International Atomic Energy Agency, Vienna, Austria.

du Toit, C., 2008. Radial variation in porosity in annular packed beds. Nuclear Engineering and Design 238, 3073–3079.

Utter, B., Behringer, R.P., 2004. Transients in sheared granular matter. The European Physical Journal E: Soft Matter and Biological Physics 14, 373–380.

Venter, P.J., Mitchell, M.N., 2007. Integrated design approach of the pebble BeD modular reactor using models. Nuclear Engineering and Design 237, 1341–1353.

Wang, D., Lu, Y., 2002. Roles and prospect of nuclear power in China's energy supply strategy. Nuclear Engineering and Design 218, 3–12.

Wang, W., Yang, X., Jiang, S., Tang, Z., Liu, Z., 2013. Numerical simulation on friction coefficient effect of pebble flow dynamics in two-dimensional pebble-bed reactor. Atomic Energy Science and Technology 47, 1141–1145.

Wu, Z., Lin, D., Zhong, D., 2002. The design features of the HTR-10. Nuclear Engineering and Design 218, 25–32.

Xu, Y., Zuo, K., 2002. Overview of the 10 MW high temperature gas cooled reactor-test module project. Nuclear Engineering and Design 218, 13–23.

Yan, W.H., Zhang, L.G., Zhang, Z., Xiao, Z.G., 2013. Feasibility studies on the burnup measurement of fuel pebbles with HPGe gamma spectrometer. Nuclear Instruments and Methods in Physics Research Section A: Accelerators, Spectrometers, Detectors and Associated Equipment 712, 130–136.

Yan, W.H., Zhang, L.G., Zhang, Z., Zhang, Y., Xiao, Z.G., 2014. Prototype studies on the nondestructive online burnup determination for the modular pebble bed reactors. Nuclear Engineering and Design 267, 172–179.

Yang, X., Hu, W., Jiang, S., Wong, K., Tu, J., 2012. Mechanism analysis of quasi-static dense pebble flow in pebble bed reactor using phenomenological approach. Nuclear Engineering and Design 250, 247–259.

Zhang, Z., Sun, Y., 2007. Economic potential of modular reactor nuclear power plants based on the Chinese HTR-PM project. Nuclear Engineering and Design 237, 2265–2274.

Zhang, Z., Wu, Z., Wang, D., Xu, Y., Sun, Y., Li, F., Dong, Y., 2009. Current status and technical description of Chinese $2 \times 250\mathrm{MW}_{\mathrm{th}}$ HTR-PM demonstration plant. Nuclear Engineering and Design 239, 1212–1219.